REPORT DOCUMENTATION PAGE

Form Approved
OMB No. 0704-0188

1. AGENCY USE ONLY (Leave blank)	2. REPORT DATE	3. REPORT TYPE AND DATES COVERED
	September 1994	Technical

4. TITLE AND SUBTITLE

Visualization of a Buried Organic Interface by Imaging TOF-SIMS and Scanning Auger Microprobe of an Ion Beam Crater Edge

5. FUNDING NUMBERS

GN0001493310058

6. AUTHOR(S)

Patrick C. Schamberger, Gary L. Jones, Joseph A. Gardella, Jr., Patrick J. McKeown, and Larry E. Davis

7. PERFORMING ORGANIZATION NAME(S) AND ADDRESS(ES)

Department of Chemistry, NSM Complex
State University of New York, University at Buffalo
Buffalo, NY 14260-3000

8. PERFORMING ORGANIZATION REPORT NUMBER

95-02

9. SPONSORING / MONITORING AGENCY NAME(S) AND ADDRESS(ES)

Department of the Navy, Office of Naval Research
800 North Quincy Street, Arlington, VA 22217-5660

10. SPONSORING / MONITORING AGENCY REPORT NUMBER

11. SUPPLEMENTARY NOTES

12a. DISTRIBUTION / AVAILABILITY STATEMENT

This document has been approved for public release and sale, its distribution is unlimited.

12b. DISTRIBUTION CODE

13. ABSTRACT (Maximum 200 words)

A method has been developed for chemically imagining a buried organic interface of thickness similar to that of a biological conditioning film. Using an ion beam to form a sputter crater, elemental analysis of the edge of the crater is performed using Auger Electron Spectroscopy (AES) and chemical imaging of the edge is performed by Time-of-Flight Secondary Ion Mass Spectrometry (TOF-SIMS). The crater edge that is formed due to the shape of the ion beam and geometry of the spectrometer has the ability to magnify the interfaces by 1000x. Samples mimicing titanium bone implant protheses were analyzed to demonstrate the feasibility of the method.

14. SUBJECT TERMS

15. NUMBER OF PAGES
56

16. PRICE CODE

17. SECURITY CLASSIFICATION OF REPORT	18. SECURITY CLASSIFICATION OF THIS PAGE	19. SECURITY CLASSIFICATION OF ABSTRACT	20. LIMITATION OF ABSTRACT
Unclassified	Unclassified	Unclassified	UL

OFFICE OF NAVAL RESEARCH

GRANT N0001493310058

R&T Code 4132083

Technical Report No. 2

Visualization of a Buried Organic Interface by Imaging TOF-SIMS and Scanning Auger Microprobe of an Ion Beam Crater Edge

by

Patrick C. Schamberger, Gary L. Jones, Joseph A. Gardella, Jr.,
Patrick J. McKeown, and Larry E. Davis

Prepared for Publication

in the

Journal of Vacuum Science and Technology A

State University of New York at Buffalo
Department of Chemistry
Buffalo, NY

September 1994

Visualization of a Buried Organic Interface by Imaging TOF-SIMS and Scanning Auger Microprobe of an Ion Beam Crater Edge

by

Patrick C. Schamberger[a], Gary L. Jones[b], Joseph A. Gardella, Jr.[a,b,*]
Natural Sciences and Mathematics Complex
Departments of Chemistry[a] and Biomaterials[b]
SUNY at Buffalo
Buffalo, NY 14260-3000

Patrick J. McKeown, Larry E. Davis
Physical Electronics
6509 Flying Cloud Drive
Eden Prairie, MN 55344

submitted to the Journal of Vacuum Science and Technology A
September 1994

* Author to whom correspondence should be addressed

ABSTRACT

A method has been developed for chemically imaging a buried organic interface of thickness similar to that of a biological conditioning film. Using an ion beam to form a sputter crater, elemental analysis of the edge of the crater is performed using Auger Electron Spectroscopy (AES) and chemical imaging of the edge is performed by Time-of-Flight Secondary Ion Mass Spectrometry (TOF-SIMS). The crater edge that is formed due to the shape of the ion beam and geometry of the spectrometer has the ability to magnify the interfaces by 1000x. Samples mimicing titanium bone implant protheses were analyzed to demonstrate the feasibility of the method.

I. INTRODUCTION

Understanding the composition at the interfaces between cells such as osteoblasts and osteoclasts, glycoproteinaceous biological conditioning films, and their metallic implants is of critical importance, for example, when strong adhesion of bone to an implant is necessary to assure reliable long term use. Without such attachment, the mechanical forces exerted on the implant can cause loosening of the implant and implant failure.[1] In order to study these interfaces, methods to determine the elemental and molecular composition of the conditioning film between implant and tissue needs to be developed. Such methods must include means by which a buried set of interfaces (cell tissue/ conditioning film and conditioning film/biomaterial) can be exposed for subsequent analysis or analysis *in situ*. Since conditioning films are on the order of magnitude of hundreds of Ångstroms[2], the technological based limits of spatial resolution of various imaging techniques add difficulties in visualizing the film between the base material and cellular overlayer. A method which can magnify the dimensions of interfaces will be advantageous in that it will be less challenging to find the position of the interfaces and avoids spacial resolution considerations for imaging if the magnification is sufficient. This paper presents the results obtained from model systems demonstrating a method that can be utilized to study the interfaces involving conditioning films. The method relies on a sputter ion erosion

technique to create a crater with a gradually sloping edge through the interfaces. The crater edge exaggerates or magnifies the dimension of the interfaces which can then be analyzed for elemental composition by Auger Electron Spectroscopy (AES) and imaged for molecular composition by Time-of-Flight SIMS (TOF-SIMS).

In addition to providing information to describe the molecular composition of a material surface, TOF-SIMS can provide images using microfocused primary ion sources or secondary ion focusing[3]. The compositions of grain boundaries, material phase domains, the results of chemical patterning/lithography, and particle inclusions all exemplify the variety of topics that can be studied by imaging TOF-SIMS[3]. Cross-sectioned interfacial analysis can also be performed to determine the properties of buried interfaces. For interfaces of materials that can easily machined, microtoming, angle lapping and ball cratering are all techniques widely used to expose and magnify dimensions of an interface[4]. Artifacts from the machining process (e.g. smearing) can be introduced if the materials do not machine well. This is expected to be the case for most organic films on a material surface. Rather than machine cut such a sample, ion erosion can be employed as a method to expose an organic film/material interface.

Crater-edge analysis from sputter ion depth profiling is commonly employed to expose a buried interface in AES[4]. However, the electron beam used in AES can severely damage an organic film during analysis[5]. It is expected that one advantage of using TOF-SIMS for organic interfaces is its low ion dosage, which minimizes sample damage during data acquisition[6]. The goal of the present study is to demonstrate the magnification power of crater edge analysis and the ability of TOF-SIMS to chemically image exposed buried organic interfaces.

The model systems used to develop the method are designed to mimic a metal implant/

conditioning film/bone tissue system. One metal of interest is titanium which has been widely used as an implant material in human bone for dental and orthopedic protheses[7]. Titanium is known to osseointegrate or sustain contact with bone when implanted[8]. Surface analytical studies of titanium implant materials studying the effects of surface preparation prior to implantation have been published[8,9]. Other metals used for bone implant protheses have also been characterized by surface analytical techniques. Co-Cr-Mo alloy was also studied as a function of treatments used before implantation[10,11]. Through discussions on the topics of osseointegration, methods used for obtaining a viable bone implant, bonding implants to bone, *in vitro* experiments on implant materials, and the use of ceramic coatings to obtain osseointegration have been published[1,12].

II. EXPERIMENTAL

A. Samples and Sample Preparation

Six types of samples were produced and are shown diagrammatically on Figure 1. Silicon wafers had a thermally grown oxide layer. The thickness was determined by ellipsometry. These were donated by Dr. Roland Chin of Intel Corporation, Portland Oregon. The Formvar films were deposited by floating a solution of Formvar (Ladd Research Industries Inc., Burlington, VT) on water and dragging the substrate through the film. The evaporated carbon overlayer was formed by vacuum evaporating a layer of graphitic carbon onto the surface in a vacuum evaporation chamber. The system employed was a Denton Vacuum DV-502 Vacuum evaporator. The system has a base pressure of 5×10^{-6} torr and operates at approximately 5×10^{-3} torr during evaporation. Carbon from a graphite rod was evaporated on the samples using a 25

amp current for 5 seconds through the graphite. The gold film was formed passing a 25 amp current through a gold sample in a sample evaporation basket for 2 seconds under similar conditions in the evaporator.

Disks two centimeters in diameter of 316L Stainless Steel (Earle M. Jorgensen, Co., Seattle, WA) and titanium (Nobelpharma USA, Chicago, IL) were polished with polishing pastes of diamond polishing compounds (Metadi II, Buehler, Lake Bluff, IL) of progressively finer grits starting with 45 micron diamond paste and finishing with 0.3 micron diamond paste. The samples were then ultrasonically cleaned for 5 minutes in baths of methanol, chloroform and tetrahydrofuran. A Polaroid gelatin film coater used to protect Polaroid photographs was used to form the model conditioning film hereafter referred to as "the gel film". The gel film was cast by dissolving several drops of the gelatin film coater material in acetone to make a saturated solution. Next, the solution was added dropwise to the sample surface and allowed to dry. Addition of the solution was halted after a film that formed a rainbow colored interference pattern was observed. The human blood film was formed by dabbing a few drops of blood from an accidental wound of the author's hand onto the metal surface. The surface was then wiped with triply distilled water to remove thick clots that had formed. Next, the surface was wiped with hexane until a film showing similar rainbow interference colors appeared. The thickness of the films was determined by a sputter depth profile experiment described below.

The calcuim hydroxyapatite [$Ca_{10}(OH)_2(PO_4)_6$] overlayer, hereafter referred to as "the HAP film" was provided as a generous donation by Dr. Catherine Cotell at the Naval Research Labs. The HAP film was applied to the substrates by pulsed laser deposition (PLD). The PLD technique for deposition of HAP films and other calcium phosphate ceramics has been published

in detail[13,14]. For the samples analyzed in this chapter, targets of calcium hydroxyapatite were produced by Seattle Specialty Ceramics (Seattle, WA). The deposition chamber was a stainless steel vacuum chamber, which was evacuated to 5×10^{-5} torr. The substrate was positioned on a stage normal to the target pellet at a distance of 8.5 cm. Films were deposited at ambient temperature. The beam from a KrF (248 nm) excimer laser operating at 25 Hz with an energy of 375 mJ/pulse was focussed on the pellet which was rotated such that the laser beam was effectively rastered over its surface to an energy density of 2 J/cm^2 at a 45° angle of incidence. The films were deposited using 65,500 pulses of the laser.

B. Film thickness determination by sputter depth profiling

The gel film thickness and blood film thickness was determined by performing a sputter depth profiling experiment using an Electron Spectroscopy for Chemical Analysis (ESCA) spectrometer. The instrument employed was a Surface Science Instruments SSX-206 ESCA. The instrument has a monochromatized Al Kα focussed x-ray source operated at 100 watts (10 mA, 10 kV) with a base pressure typically 3×10^{-10} torr and an operating pressure of 5×10^{-8} torr (2×10^{-7} torr when sputtering). A 600 micron X-ray spot size was used for the analysis. The Ti 2p region and N 1s region were used to indicate the substrate and film respectively and collected using resolution 3, a 100 eV pass energy. The depth profile crater was formed using a 4 x 4 mm raster area with a 10 mA emission current, 5 kV argon ion source. A sputter rate of 200 Å/min was determined by calibration with an Si/SiO_2 sputter depth standard. For organic materials, this translates to a sputter rate of 63Å/ min (PMMA sputters at 550Å/ min when SiO_2 sputters at 350 Å/ min)[15]. Based on these measurements, the gel film was determined to be 630Å thick and the

blood film 500Å thick. Both of these films are of a thickness approximately similar to typical conditioning films.

The elements of titanium and nitrogen were used as indicators of the metal sample and the film. When the nitrogen signal disappeared and the titanium signal was observed, one would know that complete sputtering through the film had occurred. Based on the time it took to sputter through the film, a thickness could be determined by converting sputter time to sputter depth based on a sputter depth standard. The ion gun was calibrated to an SiO_2 sputter standard and was etching the surface at a rate of 40 Å/minute. As noted above, when SiO_2 sputters at 350 Å/min, poly(methylmethacrylate) (PMMA) sputters at 550 Å/min[15]. PMMA is a polymer which should have similar sputtering characteristics as the gel film and blood films. By taking a ratio of the sputter rates, one determines that at 40 Å/min of SiO_2 sputtering, PMMA, and therefore the gel and blood films, sputter at 63 Å/min. The gel film was sputtered through in 600 seconds and the blood film in 480 seconds corresponding to thicknesses of 630 Å and 500Å.

C. Auger Electron Spectrometer

The Auger Electron Spectrometer employed was a Perkin-Elmer, Physical Electronics Division PHI-660 SAM. The instrument base pressure is typically 4×10^{-10} torr, operated at 2×10^{-8} torr when sputtering, and 1×10^{-7} torr when sputtering with an oxygen leak. An oxygen leak was used on the samples with the HAP films to minimize the loss of oxygen from the gel film and blood film due to ion beam damage. The instrument has a LaB_6 filament operated at 3 kV, 1.8 A heater current, as an electon source. The ion gun used to form the sputter craters was a Duoplasmatron gun, operated with a 5 kV accelerating voltage, 500 micron raster, 1.3 x/y raster

ratio, argon ion source. To form a distended crater edge, the sample stage was held at a 30° tilt angle.

D. TOF-SIMS spectrometer

TOF-SIMS analysis was performed on samples 4, 5 and 6. The spectrometer employed was a Physical Electronics 7200 TOF-SIMS. The instrument has a typical base pressure of 5×10^{-10} torr and and operating pressure of 8×10^{-9} torr. A liquid metal Ga^{69} ion gun operated with a 40 ns pulse width, with an energy of 25 keV for 2×10^6 pulses was used as the source of primary ions. Images were acquired in 320 by 320 micron and 400 by 400 micron areas.

III. RESULTS AND DISCUSSION

A. Thickness standards

Sample 1 (Figure 1) was first chosen since it contained an oxide layer of known thickness of the order of magnitude of conditioning film thickness. The Si wafer also has a smooth well characterized surface. The two organic materials used as conditioning film models on samples 2 and 3 were chosen since they made films of adjustable thickness easily. Formvar contains carbon and oxygen. The gel film, a Polaroid gelatin film coating material used to protect photographs, is a better material to act as a model for a conditioning film since it has nitrogen in addition to carbon and oxygen, mimicing a protein. These sample systems were chosen to optimize the tilt angle and achieve magnification factors near 10^3x (Table I).

Auger Electron Spectroscopy (AES) results for sample 1 are shown on Figures 2 a,b. Figure 2b is an Auger depth profile where the gold, silicon, and oxygen Auger lines are monitored and

their signal intensity is plotted as a function of sputter time which is directly related to depth. This figure demonstrates the ability of Auger depth profiling to monitor elemental composition of a surface as a function of depth into the surface on a well defined sample. At 3.6 minutes the gold/ SiO_2 interface is reached, indicated by the loss of Au signal and the growth of Si and O signal. At 6 minutes, the SiO_2/Si boundary is crossed as indicated by a decrease in oxygen signal and plateauing of silicon signal.

The crater edge profile for sample 1, shown on Figure 2b, indicates that the crater edge technique can also characterize a material surface by depth. The elemental line scan, obtained by monitoring the Auger peak for a particular elemental as a function of distance traversed along a line down the crater edge, for oxygen is shown on Figure 2b. The Au, SiO_2, and Si regions of the samples can be determined by the intensity of the oxygen line. Initially there is no oxygen intensity observed in the gold region, oxygen intensity present in the SiO_2, and then the oxygen intensity disappears as one enters the Si region of the sample.

Sample 2 differs from sample 1 by the Formvar film atop the sample. Notice that the Auger depth profile (Figure 3a) can resolve the interfaces since the carbon signal disappears as the gold signal grows. The rest of the profile mimics the profile obtained for sample 1. The crater edge profile with C, O, Au, and Si, line scans superimposed on Figure 3b also indicates the interfacial positions of the sample. The carbon signal decreases at 31.5 microns as the gold signal begins to increase indicating the Formvar/gold interface. The gold/SiO_2 interface is at 51 microns due to the decrease in gold intensity and increase in oxygen intensity. Finally, the SiO_2/Si interface is reached 62.9 microns along the line that defines the line scan region, suggested by the increase in Si and decrease in O intensities. Note however, that the crater edge profile is easier to intrepret

than the depth profile, and shows more discrete, less broadened interfacial boundaries. This is inherent in the crater edge analysis, which is a continuous analysis of exposed interfaces, whereas the depth profile is a stepwise process of sputtering to expose material for analysis, followed by the material analysis, followed by more sputtering, etc. These samples illustrate the ability of the crater edge method to expose and analyze a buried film on the same order of magnitude as a conditioning film. Magnification factors for these two samples are shown on Table I.

B. Evaporated Carbon/Gel Film/316L Stainless Steel sample

The samples 3, 4, 5, and 6 shown on Figure 1 are diagrams of the models designed to mimic hard tissue/biological conditioning film/metal biomaterial interfaces. The evaporated carbon and calcium hydroxyapatate (HAP) films act as models for hard tissue bone material, the gel film and blood films represent a biological conditioning film, and the 316 L stainless steel and titanium are the implant materials. The titanium and 316L stainless steel both have native oxide layers between 100 and 200Å thick[2]. Sample 3 on Figure 1 is the least refined model for the implant system being studied. The Auger elemental line scans for carbon, oxygen, nitrogen, chromium and iron are shown on Figures 4a, 4b, 4c, 4d, and 4e respectively. The carbon line scan is not exact as an indicator for the evaporated carbon/gel film interface, since carbon is found in both of these materials. However, nitrogen is unique to the gel film and can be used to determine the position along the line being scanned.

The nitrogen line scan, shown on Figure 4c suggests that the gel film ends at 47.2 microns into the line scan. The data also suggests that the line was started at a point inside the crater

along the gel film, not on the evaporated carbon layer. This is due to the difficulty in visualizing the exposed interface from the Scanning Electron Microscopy (SEM) of the Auger spectrometer. The image contrast from secondary electron emission was poor which caused difficulty in determining where the line for the line scan should begin. It should also be noted that the gel film now only contains nitrogen and carbon. The oxygen line scan (Figure 4b) shows no detectable oxygen in the gel film region. This is likely due to ion beam damage removing the oxygen during the ion erosion sputtering process.

The oxide layer on the metal is discernable in the oxygen line scan. It is detected at 47.2 microns (where the gel film ends) and ends around 100 microns across the crater edge, the point where the oxygen signal disappears. The metals associated with the oxide layer are also observable in this region since Cr (Figure 4d) and Fe (Figure 4e) intensity is detected from 47.2 microns to the end of the line scan. The magnification factor for this sample is reported on Table I.

C. Evaporated Carbon/ Gel Film/ Titanium sample

The Auger line scans for sample 4 (Figure 1) are shown in Figures 5a, 5b, 5c, and 5d (C, O, N, Ti respectively). Interpretation of gel interfaces is complicated since the nitrogen KLL transition at 379 eV overlaps with a titanium LMM transition at 380 eV. This effect can be seen on Figure 5c. At 78.8 microns the nitrogen signal shows a dramatic rise which would suggest an increase in concentration. Notice on Figure 5d, that the titanium signal is observed to rise at 78.8 microns. The increased nitrogen intensity can therefore be explained as originating from the overlapping titanium transition, which obscures the interface between the gel and the metal oxide

surface.

Based on the changes in signal intensities of the line scans, one can also determine where the interfacial positions exist. For example, the Evaporated Carbon/ gel film interface is observed at a horizontal distance approximately 20 microns from the starting point of the line scan, based on the loss of carbon intensity (Figure 5a) and appearance of a nitrogen signal at 20 microns (Figure 5c). The carbon intensity does not disappear since there is carbon in the gelatin material. Nitrogen is unique to the gel film and is used as an indicator in the Auger analysis of the film. The thickness of the film determined by the nitrogen line scan is 59 microns. This corresponds to a magnification factor of 1000x (Table I). This figure is determined by dividing the width observed from the crater edge analysis by the height of the film. This film had an approximate vertical height of 600Å.

The TOF-SIMS images allow for the direct observation of the interfaces. Figure 6 contains three positive ion images obtained for this sample. Figure 6a is an image constructed from total positive ion signal intensity across a corner of the crater. Notice that three shades of color are discernable and labelled 1, 2, and 3. This image alone tells one that the intensity of ions is highest region 3, lower in 2, and lowest in 1. The contrast seen in the image arises from the different probabilities of ion formation suggesting that each region is a different material. When one images specific ions, each region can have its respective composition defined.

Figure 6b is a TiO^+ ion image and has a high intensity of TiO^+ ions in an area that overlaps with region 3 in the total ion map. This region is the bottom of the crater, the exposed native titanium oxide. A pure titanium layer was not observed due to the ease of oxidation of titanium. The crater was formed in the Auger spectrometer in Buffalo and likely oxidized upon transfer to

the TOF-SIMS in Minneapolis.

Figure 6c is a Na^+ ion image and has the highest intensity on Na^+ ion in an area that overlaps with region 2 in the total ion map. This region corresponds to the gel film sandwiched between the evaporated carbon and the titanium. This ion is likely due to sodium dodecyl sulfate, a surfactant normally found in the gelatin material.

For this sample, the negative ion images are easier to interpret. The negative total ion image, shown in Figure 7a, also shows three discernable regions that overlap with the three regions defined in the positive total ion image. The contrast in the negative ion image is better making the identifications regions 1, 2, and 3 easier. Again, this image arises from a difference in ion formation probability for the material that composes each region. Figure 7b is an image constructed from C^- and CH^- ions summed together. The highest intensity is in an area encompassing regions 1 and 2, indicative of the elemental carbon present in the evaporated carbon and gel films. The sulfate distribution, shown in Figure 7c as an image derived from co-adding ion peaks at m/z 80, 96, and 97, is localized in an area that defines region 3. This images arises from the sodium dodecyl sulfate (SDS) in the gelatin. Since this material is a surfactant, a small amount may be leaching from the gel film and lowering the free energy of titanium by coating the metal.

A possible explanation for observing a higher intensity of sulfate ions on the titanium portion of the crater, while the counter ion (Na^+) is clearly shown at higher intensities in the gel is the relative ease of secondary ion formation from a conducting sample. The reason the low intensity of sulfate ions in the gel film region of the crater is most likely due to the difficulty in forming negative secondary ions from an insulating material, namely the organic gel film. The sodium

from the SDS is observed in the gel film region and, to a small extent, on part of the titanium portion of the crater. This overall picture suggests a small concentration of SDS leaching from the gel film to the titanium surface, but giving a high sulfate ion intensity.

Figure 7d is the most telling image of the collection. The CN^- ion is unique to the gel film, a compound that contains carbon, oxygen, and nitrogen. The highest intensity of ions is confined to an area defined by region 2, identifying region 2 as the gel film. The line shown on the figure is 60 microns across in scale, corresponding to the distance of the line scan (20 to 79 microns is 59 microns across) for detected nitrogen in the Auger (Figure 5c). The CN^- ion image allows for the direct observation of the gel film, by chemically imaging the film with an ion unique to the gel material. This result indicates that films with thicknesses of the approximate orders of magnitude (hundreds of Angstroms)[2] of conditioning films can be observed using the crater edge technique to expose the film and magnify the thickness, followed by the use of Auger Electron Spectroscopy and TOF-SIMS to visualize and analyze the film.

D. HAP/Gel Film/Titanium sample

The Auger line scans for this sample (Sample 5) are shown in Figures 8a, 8b, 8c, and 8d. As was the case for Sample 4, a difficulty arises in interpreting the data since the nitrogen KLL transition at 379 eV overlaps with a titanium LMM transition observed at 380 eV. However, carbon can be used as well as nitrogen to indicate the gel film, since the overlayer of HAP is Ca, P, and O (with H that is not observable by AES) and does not contain carbon (except as an impurity). Based on the changes in signal intensities of the line scans, one can also determine where the interfacial positions exist for Sample 5 diagrammed on Figure 1.

The HAP/ gel film interface is observed at a horizontal distance 41.2 microns from the starting point of the line scan, based on the loss of calcium intensity (Figure 8a) and appearance of a weak nitrogen signal around 41.2 microns (Figure 8c). The carbon line scan more clearly shows the gel film position. Carbon is observed on Figure 8b between 41.2 microns and 94.4 microns. The titanium portion of the crater is observed to begin at 94.4 microns across the crater edge indicated by continous intensity. It should be noted that the titanium is detected at a different position into the line scan. The peaks of the titanium in the region before 94.4 microns correspond to valleys in the carbon line scan. These features are due to sputtering irregularities caused by the HAP overlayer. The HAP film was not very smooth, as visualized by SEM, but consisted of individual particles agglomerated together to form the HAP overlayer. This material sputters slowly and can block the ion beam during sputtering and cause oscillating profiles analogous to the effect of a scratch in the metal substrate material. This effect is discussed below. The interfacial width for the gel film was determined to be 53.2 microns wide with a corresponding magnification factor of 850x (Table I).

The TOF-SIMS images obtained for this sample are shown on Figures 9 and 10. As observed for the evaporated carbon/gel film/titanium sample, the total positive ion image (Figure 9a) shows three regions of various grey intensity, but it is unclear where the gel film lies. The titanium (Figure 9b) image shown on the figure clearly illustrates where the bottom of the crater exists, the region of high ion intensity indicated by the bright region. The reverse image is observed on the Ca map (Figure 9c), where intensities are reversed compared to the Ti image. This is the HAP portion of the sample forming the rim of the crater. The gel film is indicated by the sodium ion intensity shown as a bright "C" crescent shape on the Na image (Figure 9d). This

image is due to the sodium dodecyl sulfate present in the gel film that was also observed in the evaporated carbon/gel film/ titanium sample.

The negative ion images shown on Figure 10 are inconclusive and demonstrate one difficulty of the technique. A dark band across the total ion image suggests the position of the gel film. Upon viewing images constructed from the CN^-, C_2H^- and SO_3^- ions, the position of the gel film is unclear. The CN^- intensity (Figure 10b) seen in the bottom right corner suggests the gel film is located in a region contradictory to the total ion image. This is most likely due to incomplete sputtering through the gel film to the titanium substrate. The formation of ions from a thin organic film occurs more readily than from a thicker region of the film. Therefore CN^- ions originating from the bottom of the crater where the film is thin are more readily formed than those coming from the insulating region of the thicker area of the film further out from the titanium surface along the crater edge. Additionally, it should be noted that the sample was moved and a different portion of the sample crater was imaged which can lead to a different magnification factor.

E. HAP/Blood film/Titanium sample

This sample is the most realistic model system since titanium is an actual implant material. Blood washing over the implant material at the time of implantation can form a conditioning film on the implant surface and the HAP represents the bone tissue as HAP constitutes the mineralized portion of bone[16]. The Auger line scans for this sample (Sample 6) are shown in Figures 11a, 11b, 11c, and 11d. As stated before for the other titanium samples, a difficulty arises in interpreting the data since the nitrogen KLL transition at 379 eV overlaps with a

titanium LMM transition observed at 380 eV. Again, as was the case for Sample 5, carbon can be used as well as nitrogen to indicate the blood film in Sample 6, since the overlayer of HAP is Ca, P, and O (with H that is not observable by AES) and does not contain carbon. Based on the changes in signal intensities of the line scans, one can also determine where the interfacial positions exist for this sample.

The HAP/ blood film interface is observed at a horizontal distance 35.4 microns from the starting point of the line scan, based on the loss of calcium intensity (Figure 11a) and the carbon line scan. Carbon is observed on Figure 11b between 35.4 microns and 103 microns. The titanium portion of the crater occurs from 103 microns to 118 microns across the crater edge, indicated by the plateauing of the titanium signal intensity (Figure 11d). It should be noted that the titanium can be detected before 103 microns into the line scan. The peaks of the titanium in the region before the 103 micron position correspond to valleys in the carbon line scan. These features are due to sputtering irregularities caused by the HAP overlayer. As was the case for the HAP/gel film/Ti sample, the HAP film on this sample also was not very smooth, but consisted of agglomerated particles of HAP material contributing to the oscillations observed on the line scans (see discussion below). The magnified width observed in the carbon Auger line scan is 67.6 microns with a magnification factor of 1350x (Table I).

The TOF-SIMS images obtained for this sample are shown on Figures 12 and 13. Viewing the total positive ion image on Figure 12a, it is unclear where the blood film lies since an image contrast of only two shades was obtained. However, as was the case for the other HAP coated sample, the titanium (Figure 12c) image shown on the figure clearly illustrates where the bottom of the crater exists, the region of high ion intensity indicated by the bright region in the upper

half of the image. The reverse image is observed on the Ca map (Figure 12b), where image contrast is reversed compared to the Ti image. This is the HAP portion of the sample forming the rim of the crater in the lower part of the Ca image. The blood film is indicated by the sodium ion intensity shown as a bright crescent shape on the Na image (Figure 12d).

Unlike the last sample, the negative ion images shown on Figure 13 can be used to determine the position of the blood film. For this sample, the images constructed from CN^- ion (Figure 13c) and the SO_x co-added ions (the ion intensities of the SO_3^-, SO_4^-, and HSO_4^- ions are summed to form the SO_x image) (Figure 13d) can be used to show the position of the blood film. The region of high ion intensity forms an arc from the left side to the bottom of the image outlines the corner of the crater.

F. Effect of sample morphology on Auger line scans

Morphological features such as a scratch in the metal substrate surface or a non uniformity in the HAP overlayer film can complicate intrepretation of the Auger line scan data as well as the TOF-SIMS images. Figure 14 diagrams how a scratch and a large particle on the sample surface can effect the Auger line scan. Initially, the organic film, in the case shown uses a gel film sample, can intrude into a scratch on the metal surface and fill the void as shown on the figure. Additionally, an nonuniformity of the overlaying film, in this case an HAP particle, can protrude from the surface as shown on the "before crater formation" portion of the diagram. When the crater is formed, assuming no differential sputtering rates for simplicity, a portion of the HAP particle will be left still causing a protrusion as shown designated as region 3 on the "after crater formation" portion of Figure 14. As one proceeds across the crater edge during a line scan one

passes through 8 regions as shown. The data one obtains from such a sample can be described as follows.

For simplicity, data will be collected for calcium, indicating the HAP overlayer, carbon indicating the gel film, and titanium indicating the titanium oxide layer and titanium on the crater shown. In region one, there will be high intensity of calcium, no carbon or titanium, as HAP is being detected. Passing across the HAP/Gel film interface into region 2, the calcium intensity disappears, carbon is observed and no titanium is detected. Region 3 causes the first complication of the line scan data. The carbon intensity disappears (or diminishes) and calcium reappears, as the HAP particle that was not completely removed during sputtering is passed over by the line scan. Proceeding to region 4 causes the calcium to disappear again and the carbon to reappear as we are now sampling the gel film material. This effect causes the undulations observed on the calcium, phosphorus, carbon, oxygen, and nitrogen line scans obtained experimentally.

Continuing with the scan, expected behavior of the line scan profiles is resumed. The carbon intensity disappears and now titanium is observed upon passing into region 5 crossing the gel film/titanium oxide interface. Instead of the titanium intensity increasing due to the observation of titanium metal instead of the oxide, the titanium signal disappears and carbon reappears as one enters region 6. Region 6 is the gel film material that intruded down into a scratch deep enough to not be milled off the surface during the ion erosion process. As region 7 is entered, the carbon disappears again and the titanium signal reappears since the metal oxide is being probed. This effect causes additional undulations observed on the carbon, oxygen and nitrogen line scans as well as undulations on the titanium line scans in the experimental results. Finally, the titanium

intensity increases and plateaus as one crosses into region 8, the metal with the oxide layer removed as a result of sputtering.

IV. CONCLUSION

In summary, the crater edge technique can be used to expose and magnify a buried organic interface, with less smearing than a mechanical cutting or cross-sectioning where the "hardness" of all materials must be similar to effect a good presentation of the interface, preserving its spacial integrity. Magnification factors ranging from 710x to 1350x were observed. The range is due to irregularities (i.e. scratches in the surface and particles in the overlayer) of the samples. The nitrogen content in the gel film allowed for mapping of the buried organic film by TOF-SIMS. Also, TOF-SIMS ion mass analysis will allow for more possible characteristic signals which can be used to avoid the problem of overlapping signals detected by other techniques. Lastly, the combination of positive and negative ion imaging with crater edge profiling allows for the characterization of buried organic interfaces.

ACKNOWLEDGEMENTS

The authors wish to acknowledge Dr. Catherine Cotell at the Naval Research Labs for graciously producing the calcium hydroxyapatite films. The Industry/University Cooperative Center for Biomaterials, through the National Science Foundation and NSF Polymers Program (NSF DMR 9303032) and the Office of Naval Research, Chemistry Division is acknowledged for supporting this project.

REFERENCES

[1]R.M. Pillar, J.E. Davies, D.C. Smith, Mat. Res. Soc. Bull. **16 (9)**, 55-61 (1991).

[2]A.G. Gristina, Science. **237**, 1588-1595 (1987).

[3]A. Benninghoven, B. Hagenhoff, E. Niehuis, Anal. Chem. **65 (14)**, 630A-640A (1993).

[4]H.E. Bishop, in *Methods of Surface Analysis*, edited by J.M. Walls, (Cambridge University Press, New York, 1989), p. 118.

[5]H.E. Bishop, in *Methods of Surface Analysis*, edited by J.M. Walls, (Cambridge University Press, New York, 1989), p. 100.

[6]D.M. Hercules, J. Molecular Structure. **292**, 49-64 (1993).

[7]T. Albrcktsson, P.I. Branemark, H.A. Hansson, B. Kasemo, K. Larsson, I. Lundstrom, D.H. McQueen, R. Skalak, Ann. Biomed. Eng. **11**, 1 (1983).

[8]P.I. Branemark, R. Adell, T. Albrecktsson, U. Lekholm, S. Lundkvist, B.Rockler, Biomaterials. **4**, (1983).

[9]N.L. Hernandez de Gatica, G.L. Jones, J.A. Gardella, Jr., Appl. Surf. Sci. **68**, 107-121 (1993).

[10]R.L. Moore, G.L. Grobe, III., J.A. Gardella, Jr., J. Vac. Sci. Technol. A. **9 (3)**, 1323-1328 (1991).

[11]G. Lewis, J. Vac. Sci. Technol. A. **11 (1)**, 168-174 (1993).

[12]L.L Hench, J. Wilson, Mat. Res. Soc. Bull. **16 (9)**, 62-74 (1991).

[13]C.M. Cotell, D.B. Chrisey, K.S. Grabowski, J.A. Sprague, C.R. Gossett, C.R. J. Appl. Biomaterials. **3**, 87-93 (1992).

[14]C.M. Cotell, Appl. Surf. Sci. **69**, 140-148 (1993).

[15]*Ion Beam Etch Rates Bulletin*. Commonwealth Scientific Corp.: Alexandria, VA. 1978.

[16]J.E. Huheey, *Inorganic Chemistry, 3rd edition*, (Harper and Row, New York, 1983), p. 916.

Table I: Magnification Factors

Sample	Vertical Height (Å)	Exposed Width of Crater (μ)	Magnification Factor
Gold/ SiO_2/ Si	223	26.4	1080x
Formvar/ Gold/SiO_2/ Si	223	16.0	710x
Evaporated Carbon/ Gel Film/ 316L Stainless Steel	500	47.0	940x
Evaporated Carbon/ Gel Film/ Titanium	600	59.0	1000x
HAP/ Gel Film/ Titanium	630	53.2	850x
HAP/ Blood Film/ Titanium	500	67.7	1350x

Figures and Figure Captions

Figure 1: Diagram of samples studied

Figure 2a: Auger sputter depth profile for Gold/SiO_2/Si sample

Figure 2b: Oxygen Auger line scan across crater for Gold/SiO_2/Si sample

Figure 3a: Auger sputter depth profile for Formvar/Gold/SiO_2/Si sample

Figure 3b: Oxygen Auger line scan across crater for Formvar/Gold/SiO_2/Si sample

Figure 4a: Carbon Auger line scan for Evaporated Carbon/Gel Film/316L Stainless Steel sample

Figure 4b: Oxygen Auger line scan for Evaporated Carbon/Gel Film/316L Stainless Steel sample

Figure 4c: Nitrogen Auger line scan for Evaporated Carbon/Gel Film/316L Stainless Steel sample

Figure 4d: Chromium Auger line scan for Evaporated Carbon/Gel Film/316L Stainless Steel sample

Figure 4e: Iron Auger line scan for Evaporated Carbon/Gel Film/316L Stainless Steel sample

Figure 5a: Carbon Auger line scan for Evaporated Carbon/Gel Film/Titanium sample

Figure 5b: Oxygen Auger line scan for Evaporated Carbon/Gel Film/Titanium sample

Figure 5c: Nitrogen Auger line scan for Evaporated Carbon/Gel Film/Titanium sample

Figure 5d: Titanium Auger line scan for Evaporated Carbon/Gel Film/Titanium sample

Figure 6a: TOF-SIMS total positive ion image of sputter crater on Evaporated Carbon/Gel Film/Titanium sample

Figure 6b: TOF-SIMS TiO^+ ion image of sputter crater on Evaporated Carbon/Gel Film/Titanium sample

Figure 6c: TOF-SIMS Na^+ ion image of sputter crater on Evaporated Carbon/Gel Film/Titanium sample

Figure 7a: TOF-SIMS total negative ion image of sputter crater on Evaporated Carbon/Gel

Film/Titanium sample

Figure 7b: TOF-SIMS C^-, CH^- co-added ion image of sputter crater on Evaporated Carbon/Gel Film/Titanium sample

Figure 7c: TOF-SIMS SO_3^-, SO_4^-, HSO_4^- co-added ion image of sputter crater on Evaporated Carbon/Gel Film/Titanium sample

Figure 7d: TOF-SIMS CN^- ion image of sputter crater on Evaporated Carbon/Gel Film/Titanium sample

Figure 8a: Calcium Auger line scan for HAP/Gel Film/Titanium sample

Figure 8b: Carbon Auger line scan for HAP/Gel Film/Titanium sample

Figure 8c: Nitrogen Auger line scan for HAP/Gel Film/Titanium sample

Figure 8d: Titanium Auger line scan for HAP/Gel Film/Titanium sample

Figure 9a:TOF-SIMS total positive ion image of sputter crater on HAP/Gel Film/Titanium sample

Figure 9b:TOF-SIMS Ti^+ ion image of sputter crater on HAP/Gel Film/Titanium sample

Figure 9c:TOF-SIMS Ca^+ ion image of sputter crater on HAP/Gel Film/Titanium sample

Figure 9d:TOF-SIMS Na^+ ion image of sputter crater on HAP/Gel Film/Titanium sample

Figure 10a: TOF-SIMS total negative ion image of sputter crater on HAP/Gel Film/Titanium sample

Figure 10b: TOF-SIMS CN^- ion image of sputter crater on HAP/Gel Film/Titanium sample

Figure 10c: TOF-SIMS C_2H^- ion image of sputter crater on HAP/Gel Film/Titanium sample

Figure 10d: TOF-SIMS SO_3^- ion image of sputter crater on HAP/Gel Film/Titanium sample

Figure 11a: Calcuim Auger line scan for HAP/Blood Film/Titanium sample

Figure 11b: Carbon Auger line scan for HAP/Blood Film/Titanium sample

Figure 11c: Nitrogen Auger line scan for HAP/Blood Film/Titanium sample

Figure 11d: Titanium Auger line scan for HAP/Blood Film/Titanium sample

Figure 12a:TOF-SIMS total positive ion image of sputter crater on HAP/Blood Film/Titanium sample

Figure 12b:TOF-SIMS Ca^+ ion image of sputter crater on HAP/Blood Film/Titanium sample

Figure 12c:TOF-SIMS Ti^+ ion image of sputter crater on HAP/Blood Film/Titanium sample

Figure 12d:TOF-SIMS Na^+ ion image of sputter crater on HAP/Blood Film/Titanium sample

Figure 13a: TOF-SIMS total negative ion image of sputter crater on HAP/Blood Film/Titanium sample

Figure 13b: TOF-SIMS O^- ion image of sputter crater on HAP/Blood Film/Titanium sample

Figure 13c: TOF-SIMS CN^- ion image of sputter crater on HAP/Blood Film/Titanium sample

Figure 13d: TOF-SIMS SO_3^-, SO_4^-, HSO_4^- co-added ion image of sputter crater on HAP/Blood Film/Titanium sample

Figure 14: Diagram of the effect a scratch and a large particle on a surface has on a sputter crater

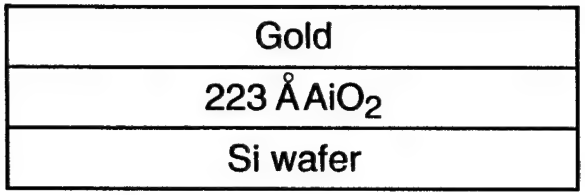
Gold
223 Å AiO_2
Si wafer

1

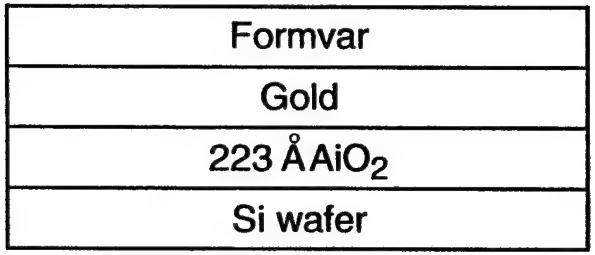
Formvar
Gold
223 Å AiO_2
Si wafer

2

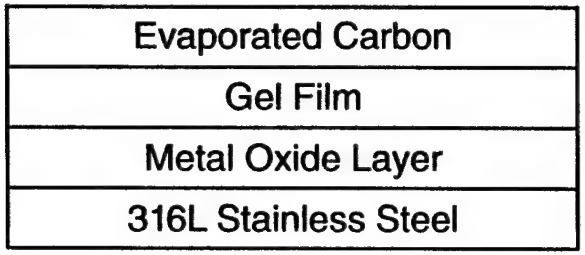
Evaporated Carbon
Gel Film
Metal Oxide Layer
316L Stainless Steel

3

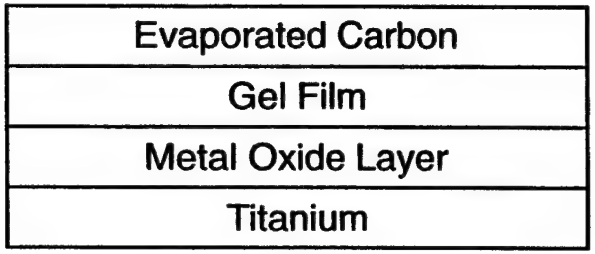
Evaporated Carbon
Gel Film
Metal Oxide Layer
Titanium

4

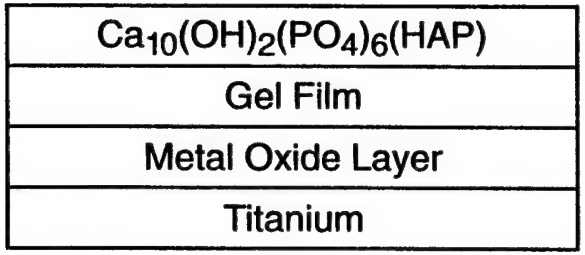
$Ca_{10}(OH)_2(PO_4)_6$(HAP)
Gel Film
Metal Oxide Layer
Titanium

5

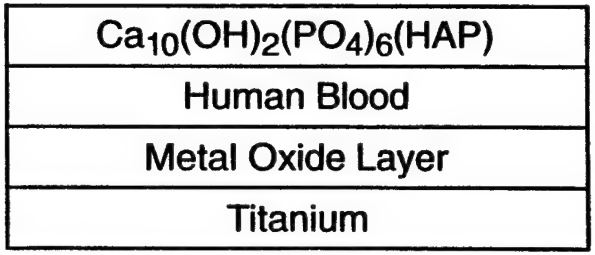
$Ca_{10}(OH)_2(PO_4)_6$(HAP)
Human Blood
Metal Oxide Layer
Titanium

6

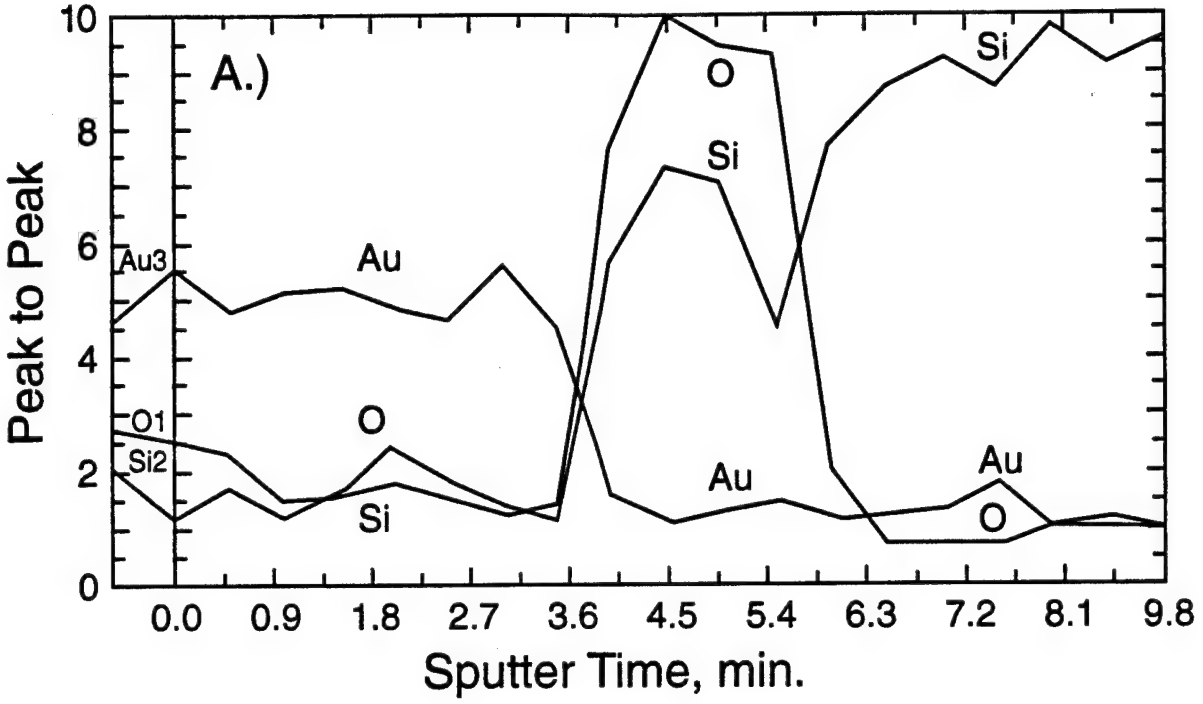
A.)
Peak to Peak
Sputter Time, min.
Au3
O1
Si2
Au
O
Si
O
Si
Au
Au
O
Si
0
2
4
6
8
10
0.0
0.9
1.8
2.7
3.6
4.5
5.4
6.3
7.2
8.1
9.8

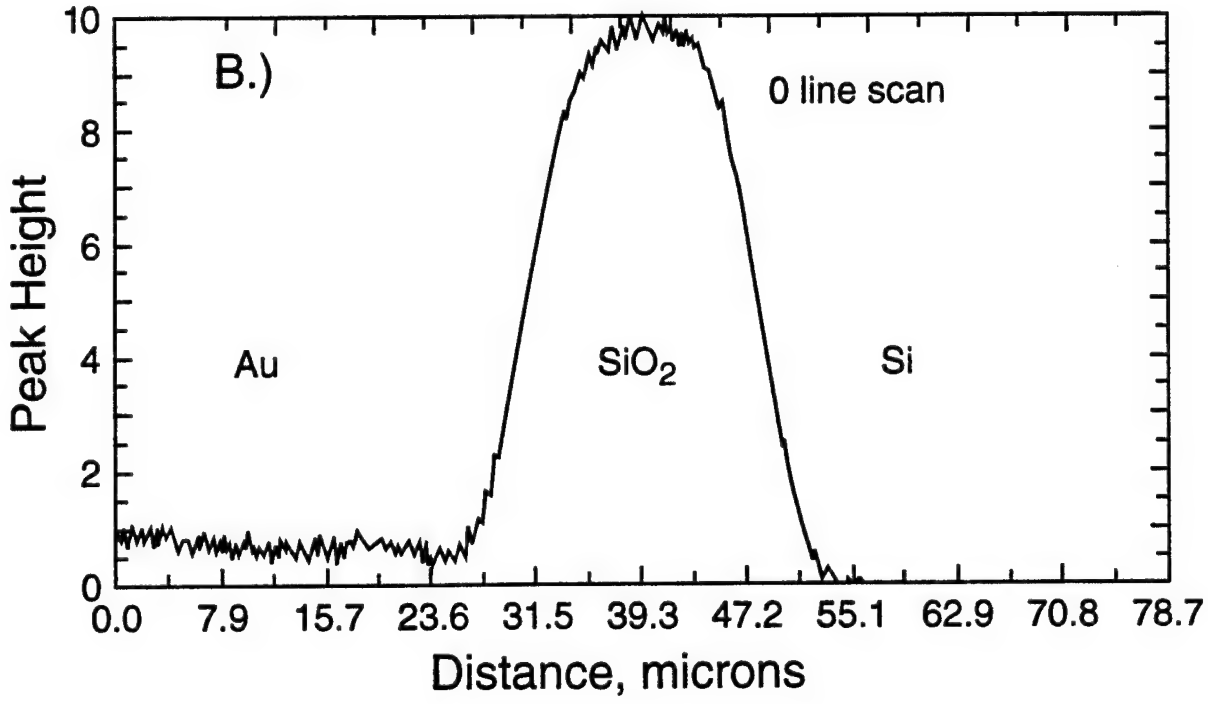
B.)
0 line scan
Peak Height
Distance, microns
Au
SiO2
Si
0
2
4
6
8
10
0.0
7.9
15.7
23.6
31.5
39.3
47.2
55.1
62.9
70.8
78.7

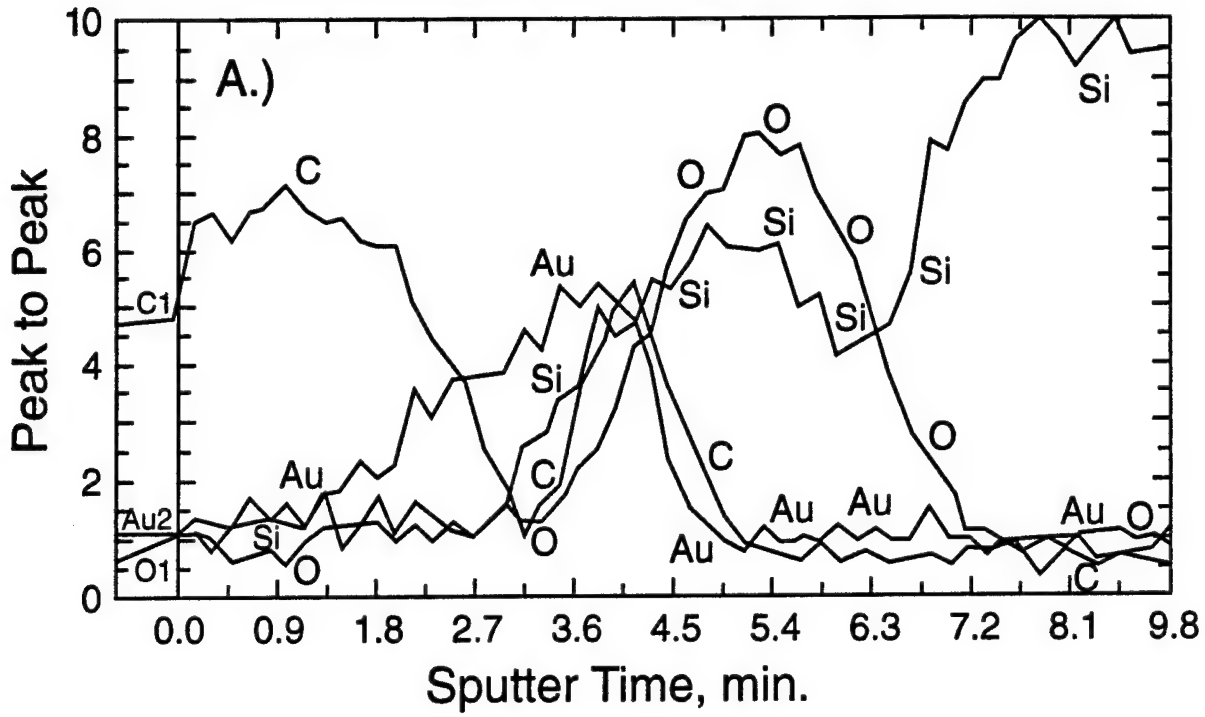
A.)
Peak to Peak
Sputter Time, min.
C1
Au2
O1
0.0
0.9
1.8
2.7
3.6
4.5
5.4
6.3
7.2
8.1
9.8

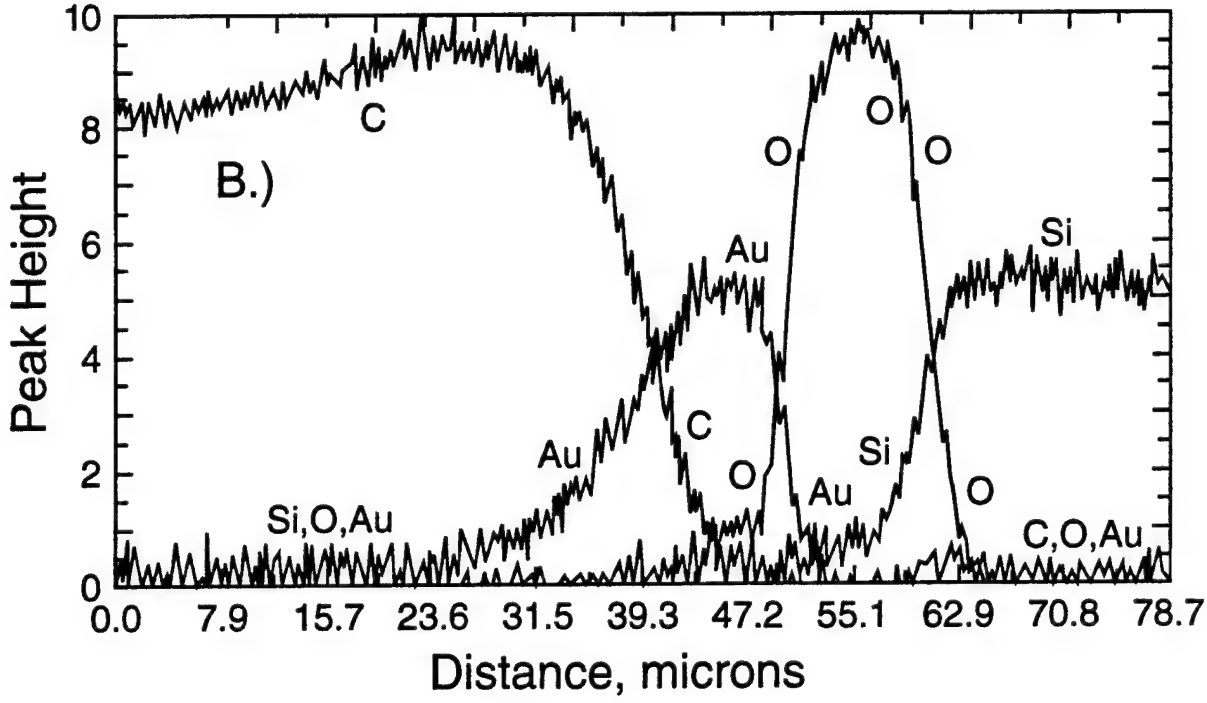
B.)
Peak Height
Distance, microns
Si,O,Au
C,O,Au
0.0
7.9
15.7
23.6
31.5
39.3
47.2
55.1
62.9
70.8
78.7

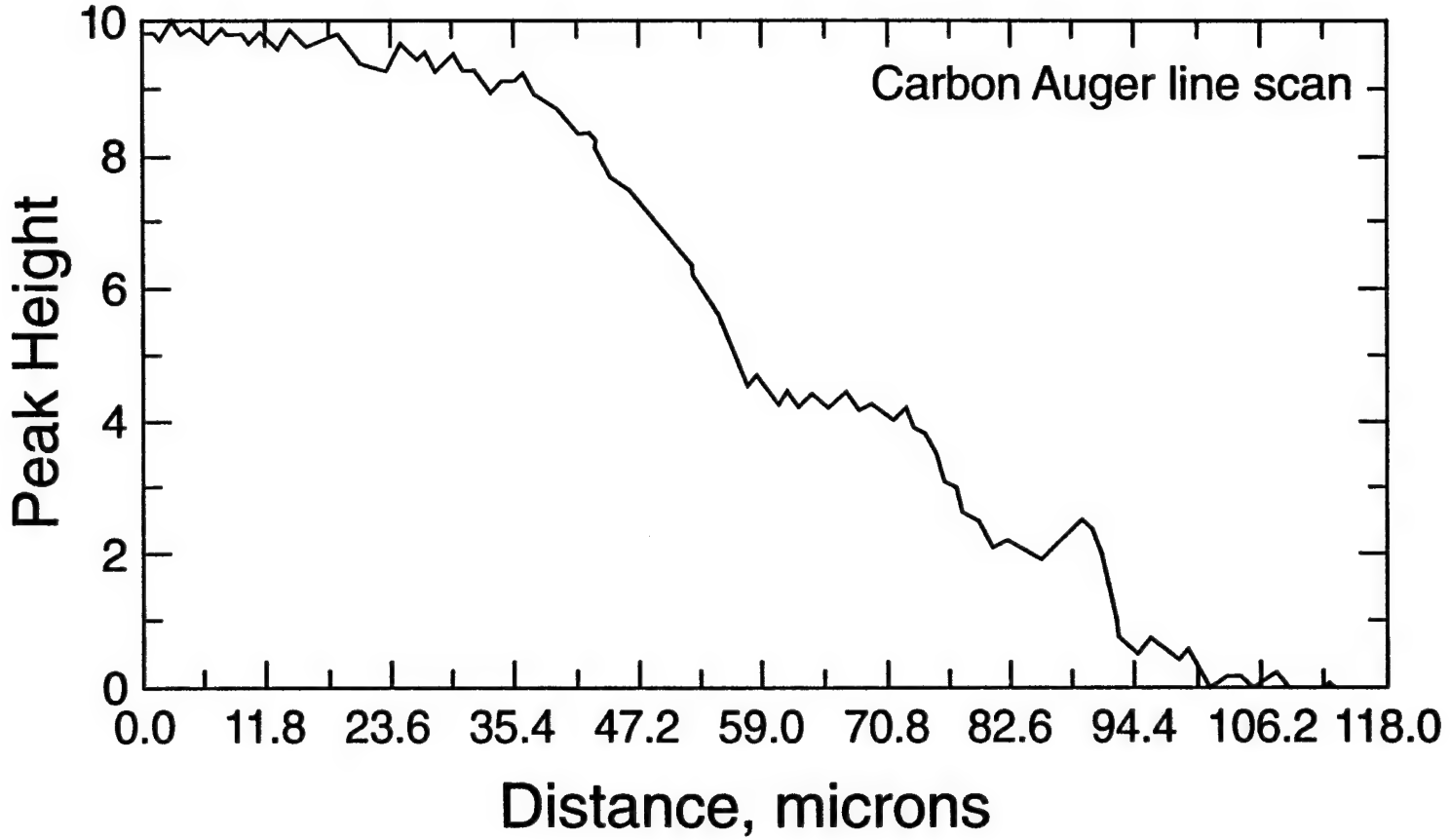
Carbon Auger line scan
Peak Height
10
8
6
4
2
0
0.0
11.8
23.6
35.4
47.2
59.0
70.8
82.6
94.4
106.2
118.0
Distance, microns

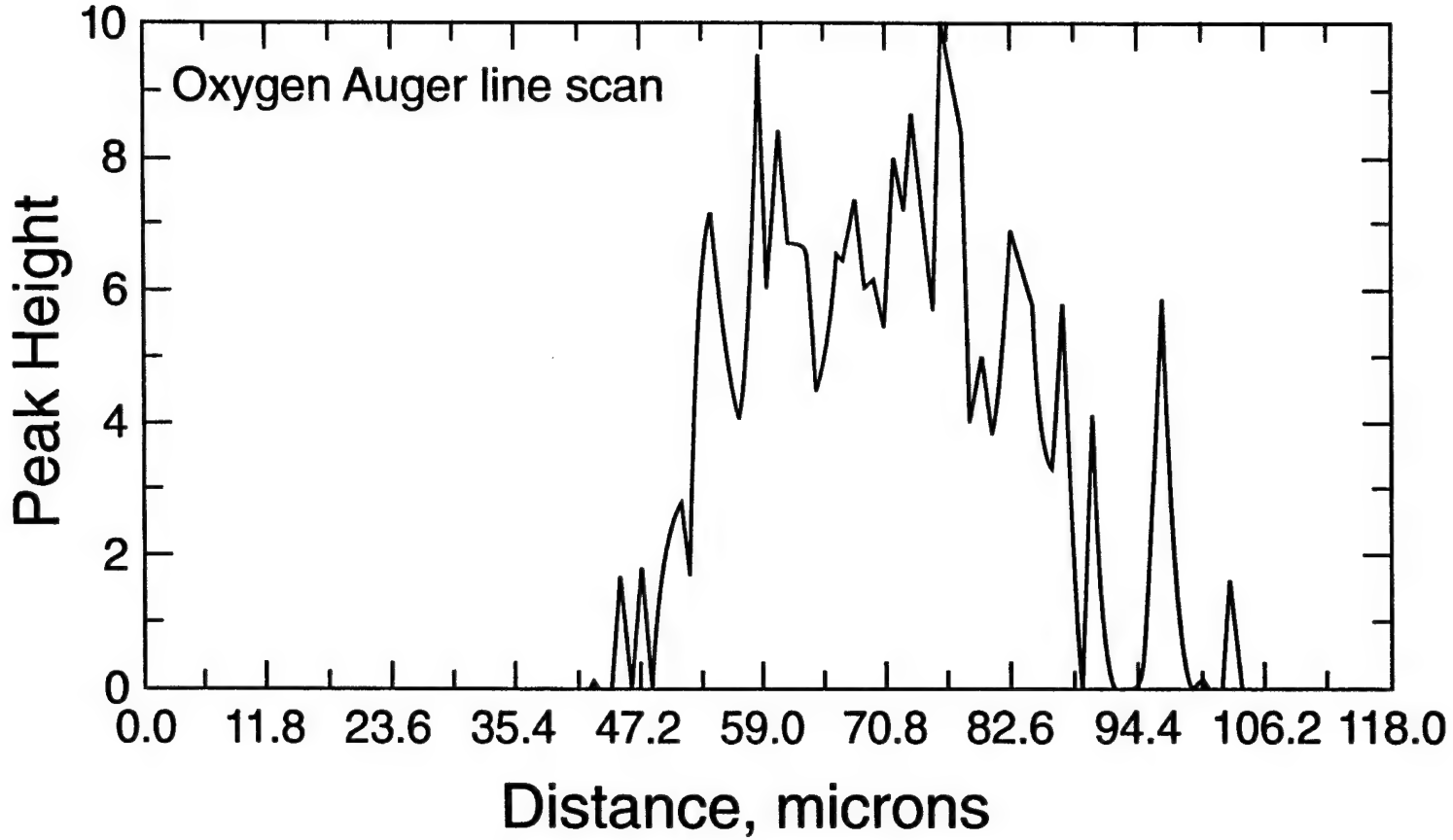
Oxygen Auger line scan
Peak Height
10
8
6
4
2
0
0.0
11.8
23.6
35.4
47.2
59.0
70.8
82.6
94.4
106.2
118.0
Distance, microns

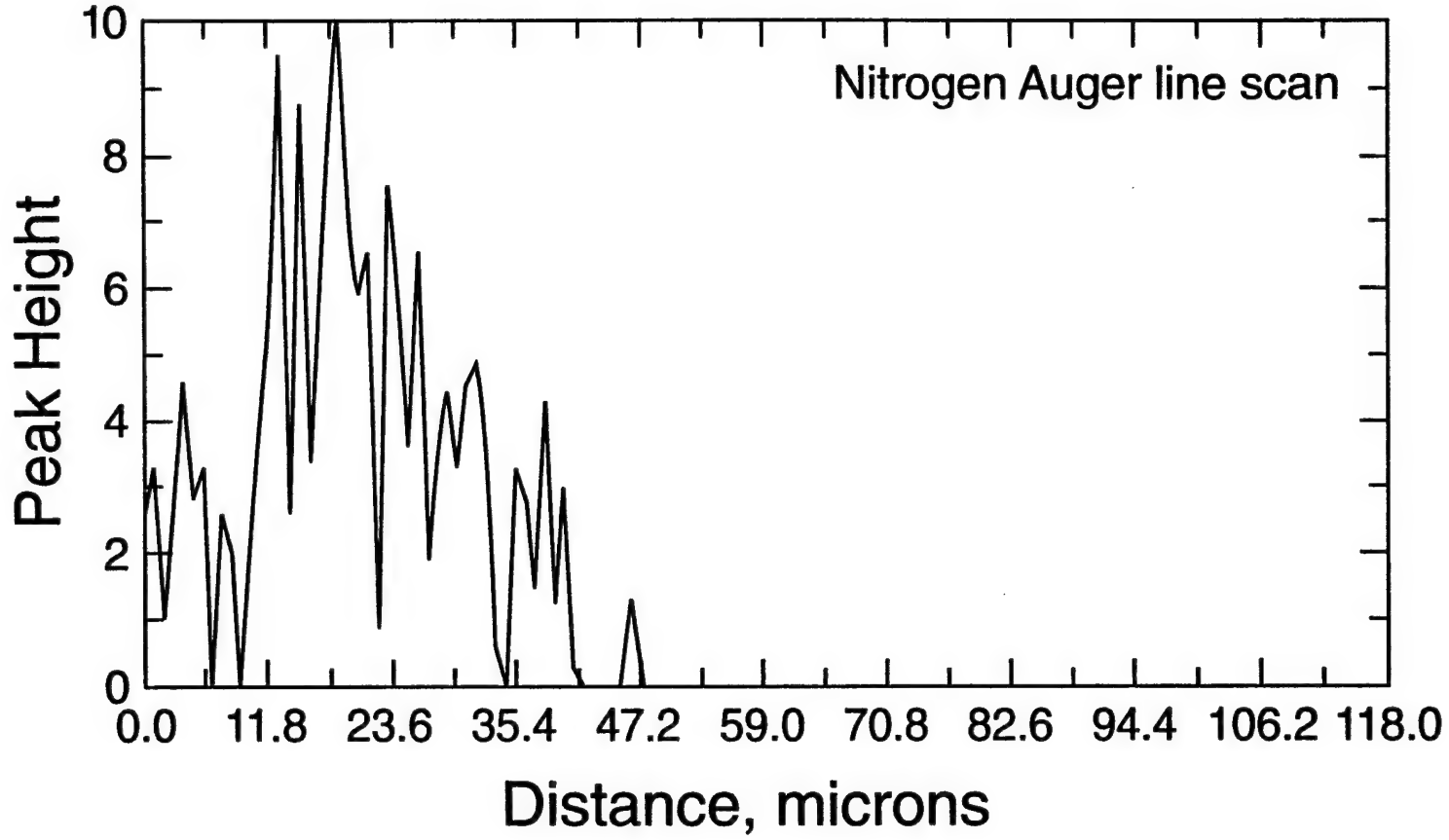
Nitrogen Auger line scan
Peak Height
10
8
6
4
2
0
0.0
11.8
23.6
35.4
47.2
59.0
70.8
82.6
94.4
106.2
118.0
Distance, microns

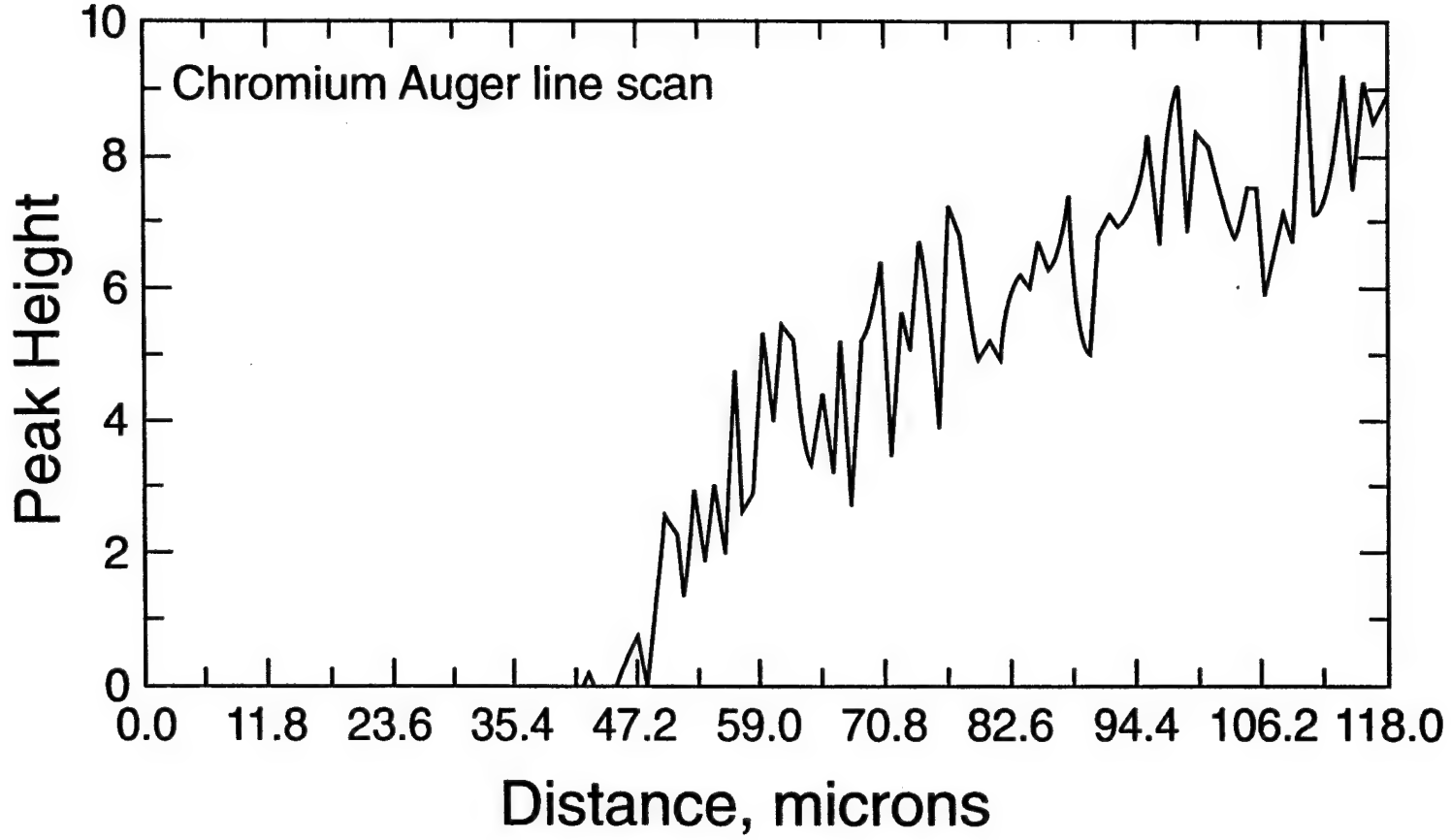

Schamberg 940363.33g

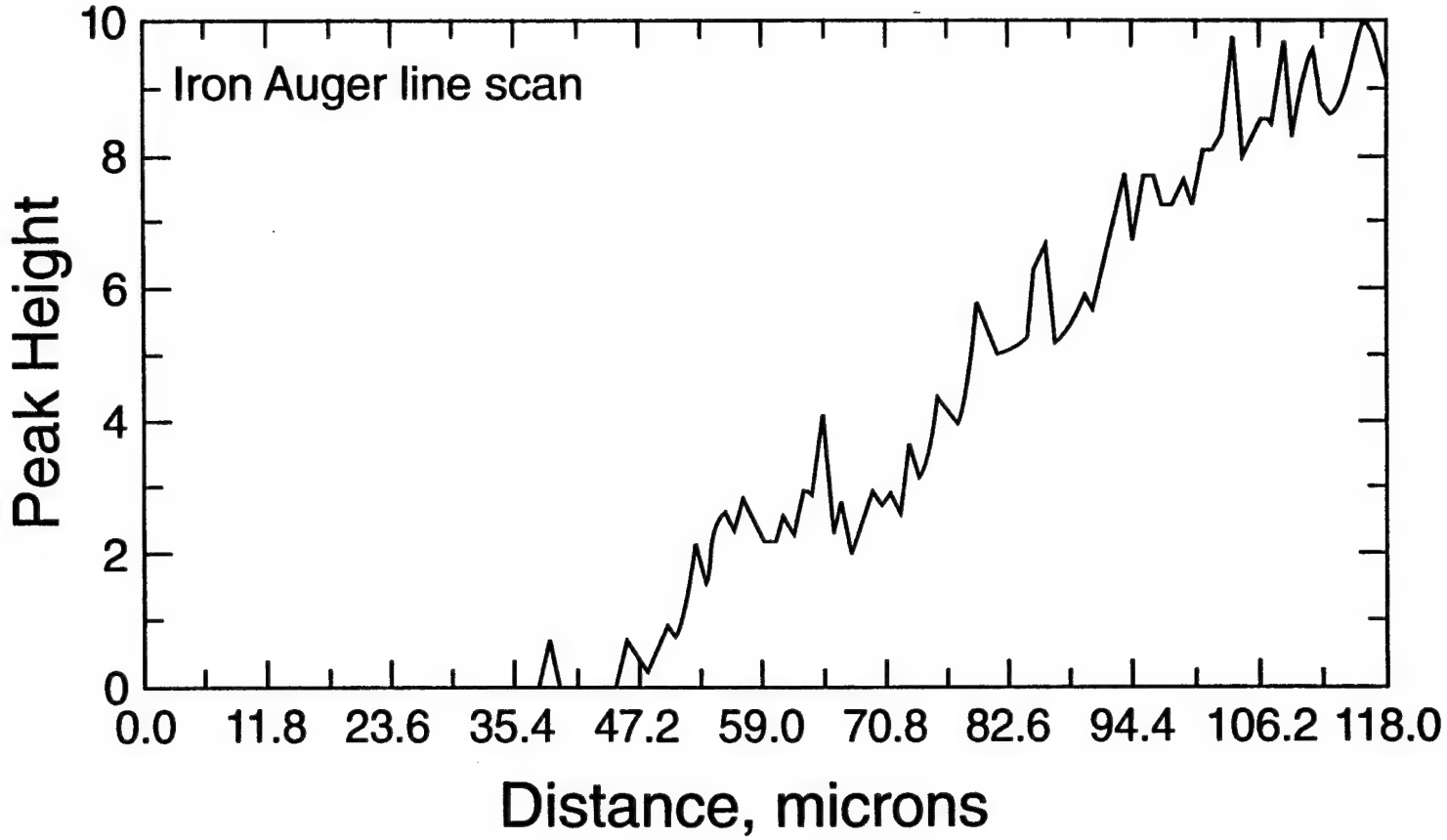

Schamberg 940363.34g

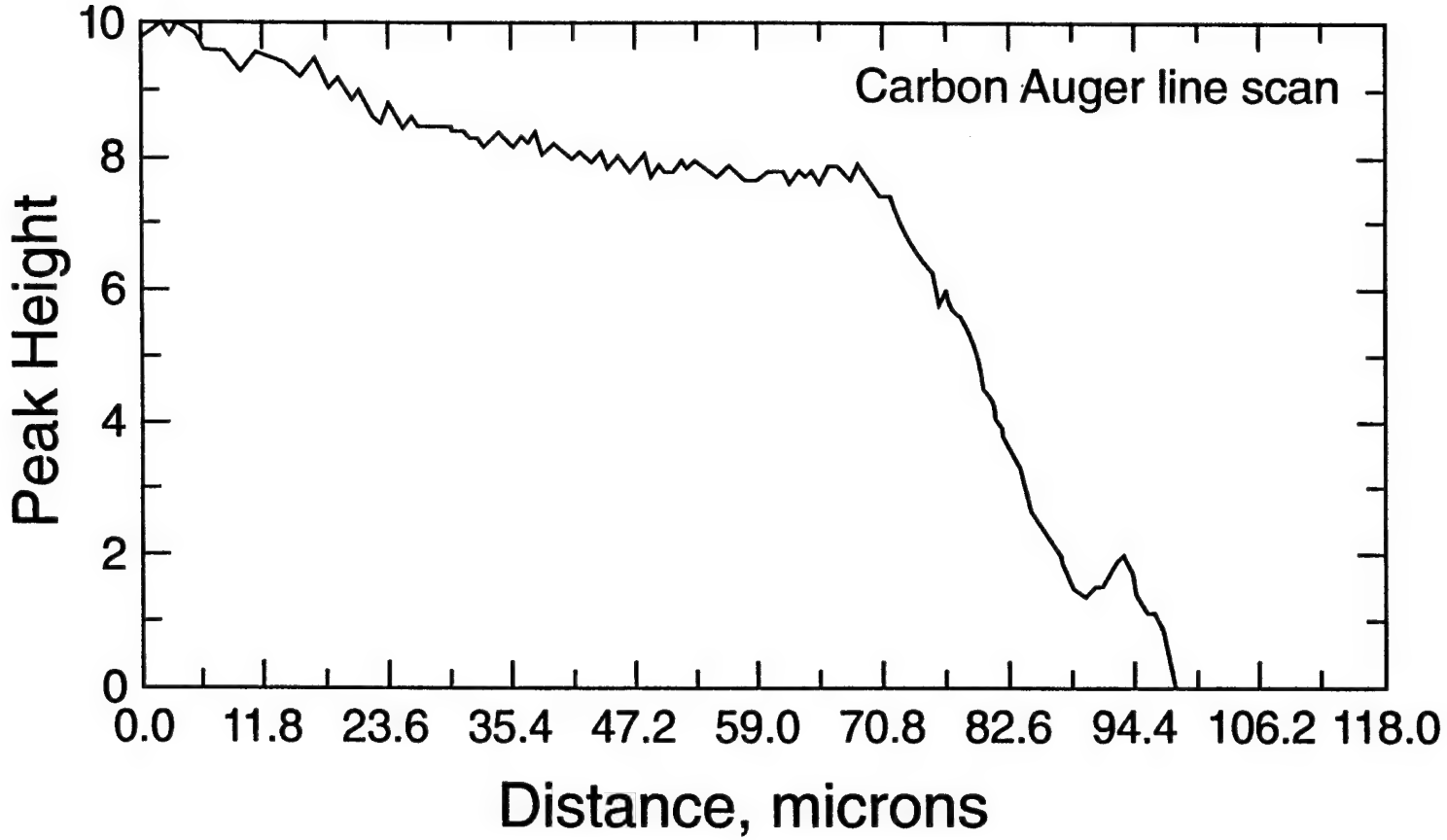
Carbon Auger line scan
Peak Height
10
8
6
4
2
0
0.0
11.8
23.6
35.4
47.2
59.0
70.8
82.6
94.4
106.2
118.0
Distance, microns

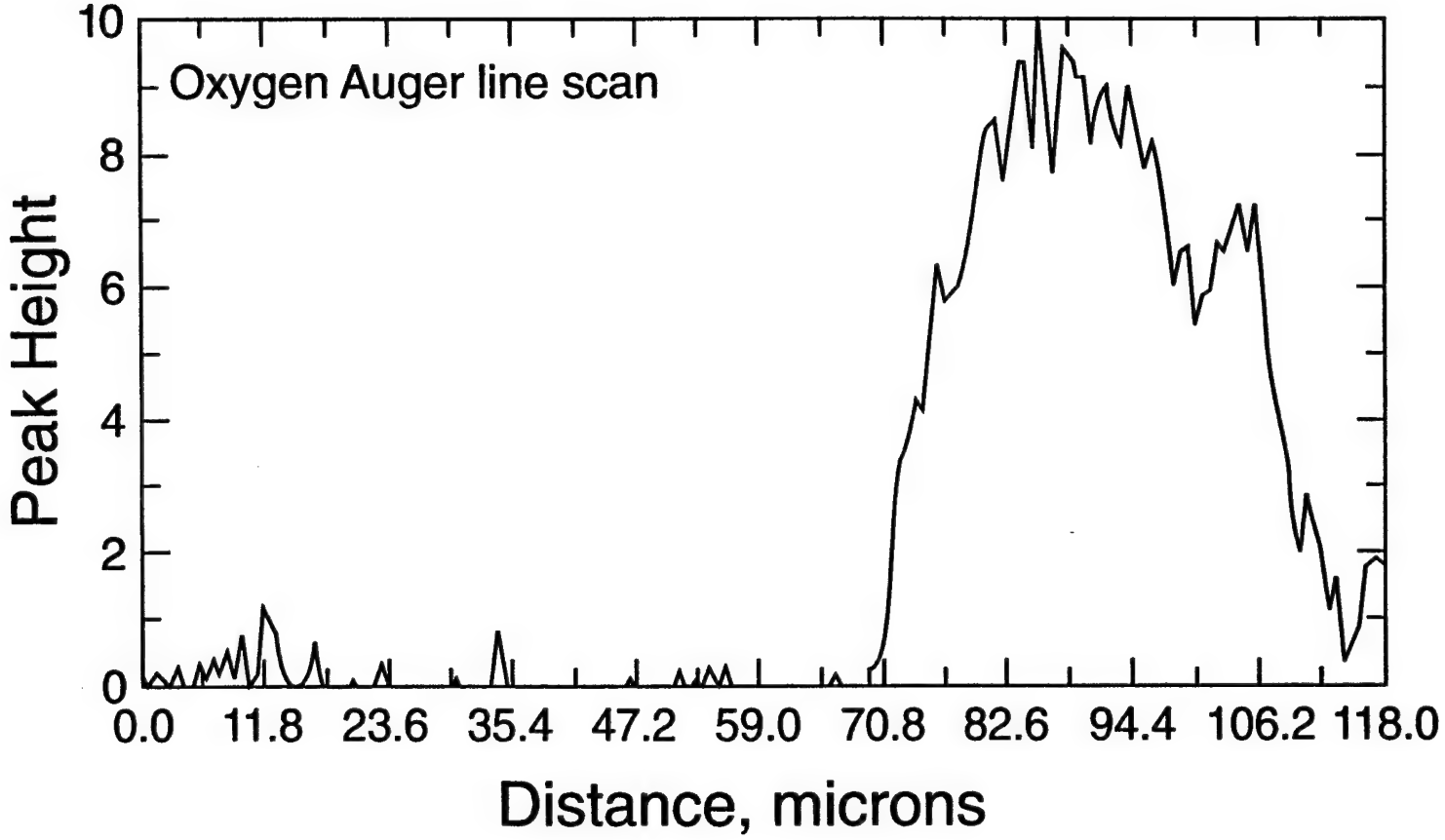
Oxygen Auger line scan
Peak Height
10
8
6
4
2
0
0.0
11.8
23.6
35.4
47.2
59.0
70.8
82.6
94.4
106.2
118.0
Distance, microns

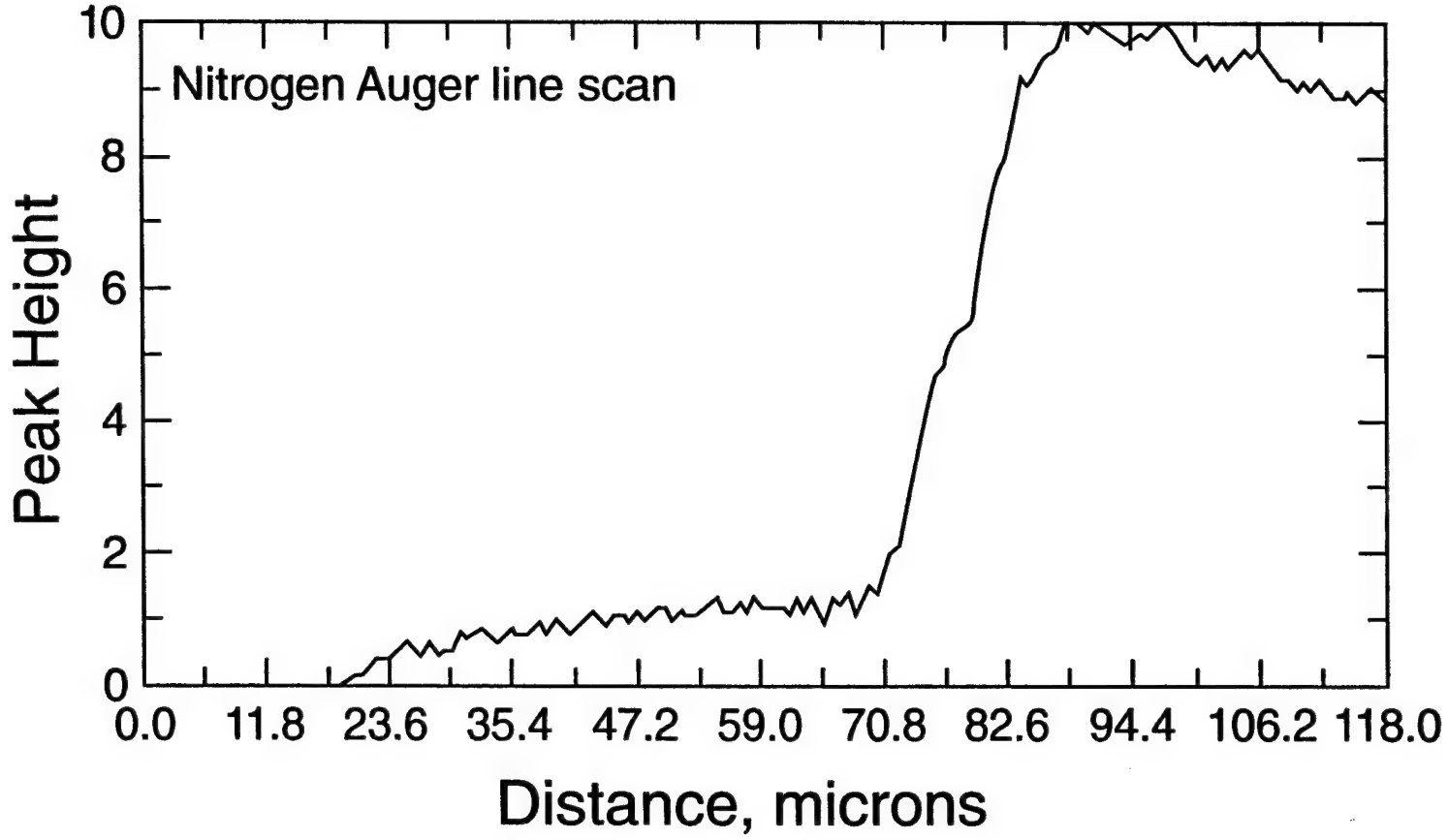

Schamberg 940363.37g

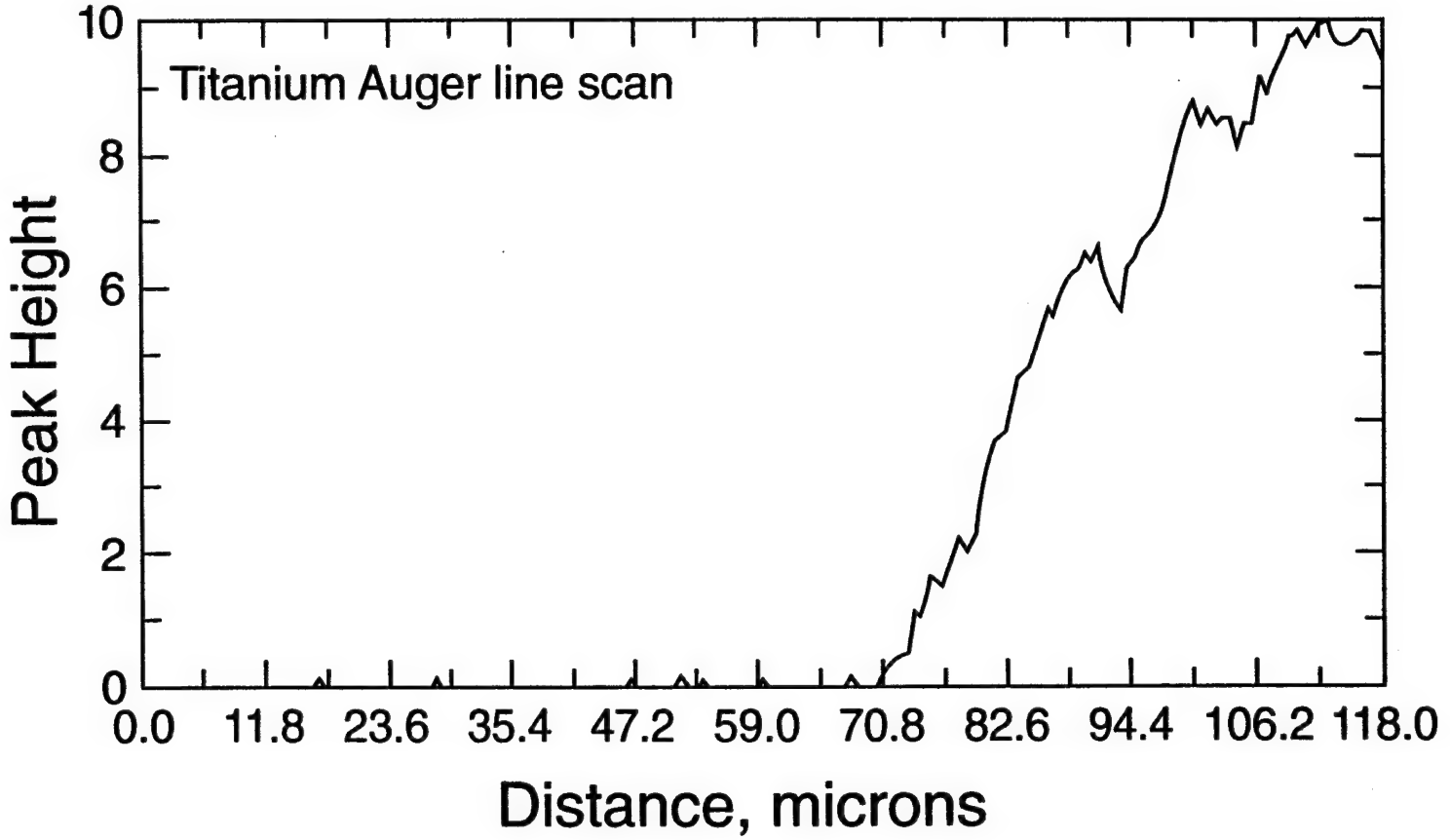

Schamberg 940363.38g

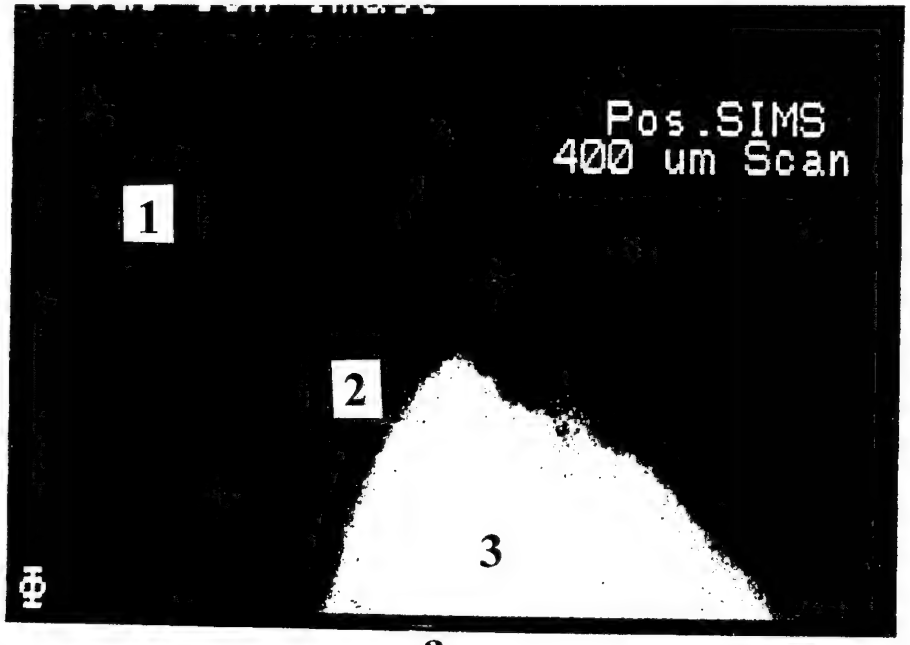
Pos.SIMS
400 um Scan
1
2
3

a


TiO Distribution (m/z 64)
Pos.SIMS
400 um Scan
3

b

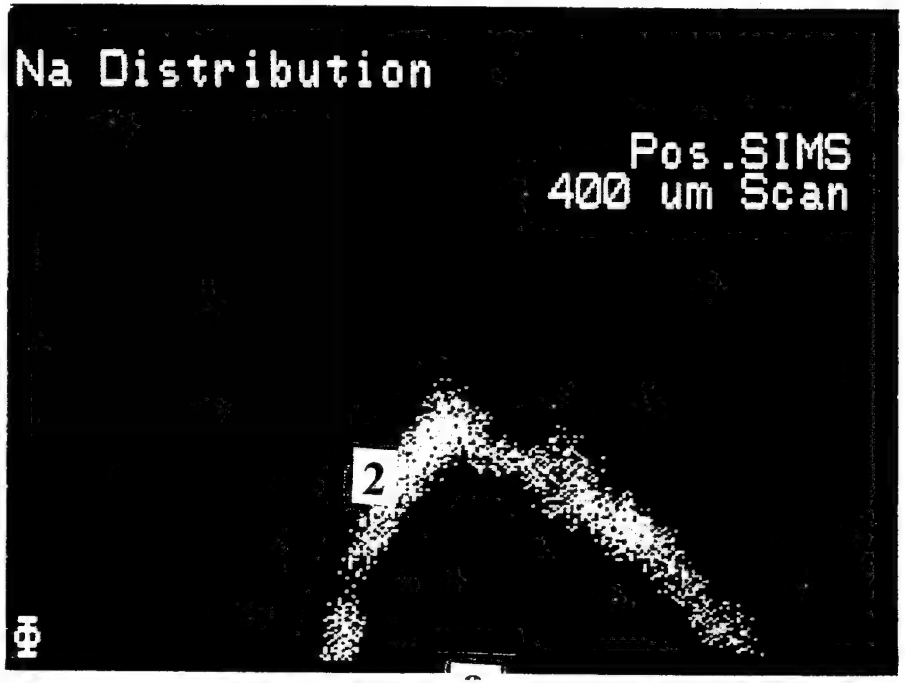
Na Distribution
Pos.SIMS
400 um Scan
2

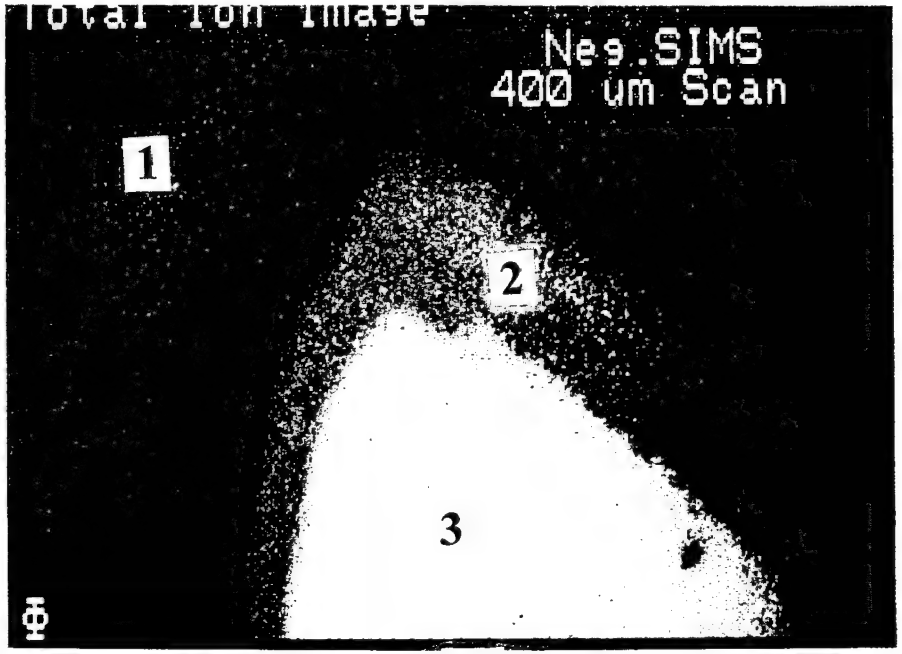
Total Ion Image
Neg.SIMS
400 um Scan
1
2
3

a

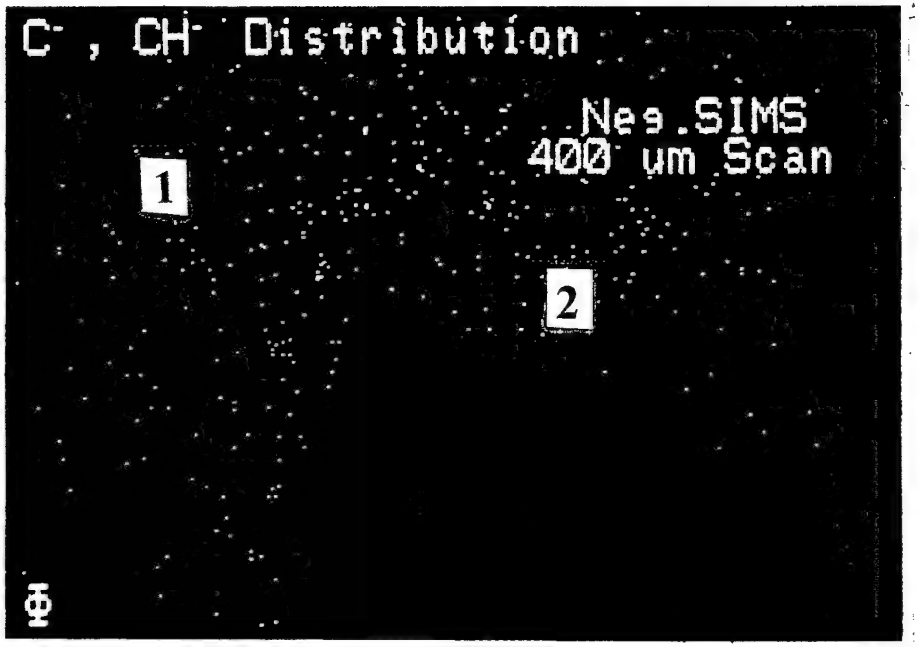
C⁻ , CH⁻ Distribution
Neg.SIMS
400 um Scan
1
2

b

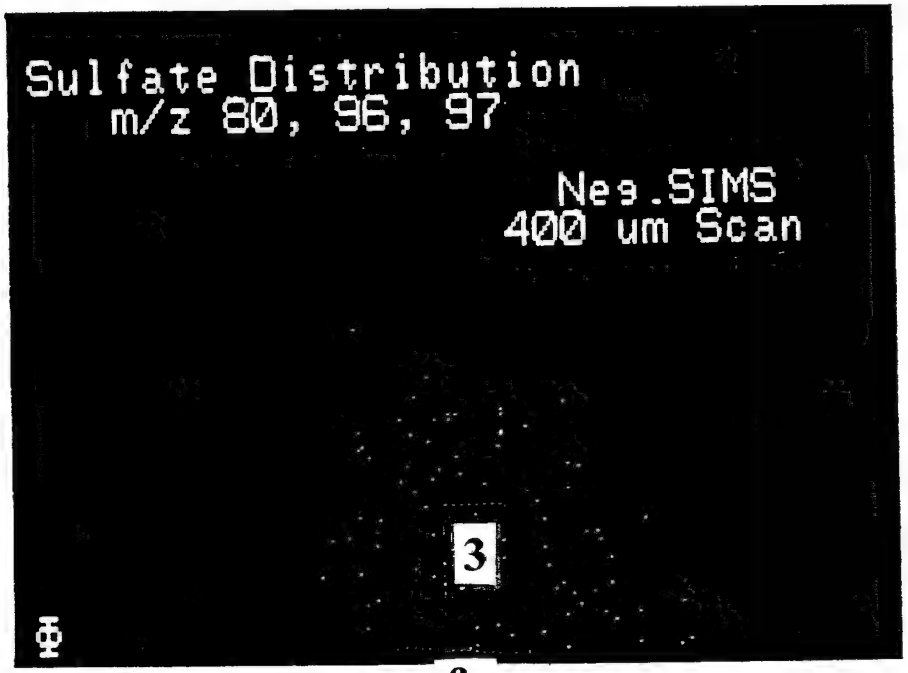
Sulfate Distribution
m/z 80, 96, 97
Neg.SIMS
400 um Scan
3

c

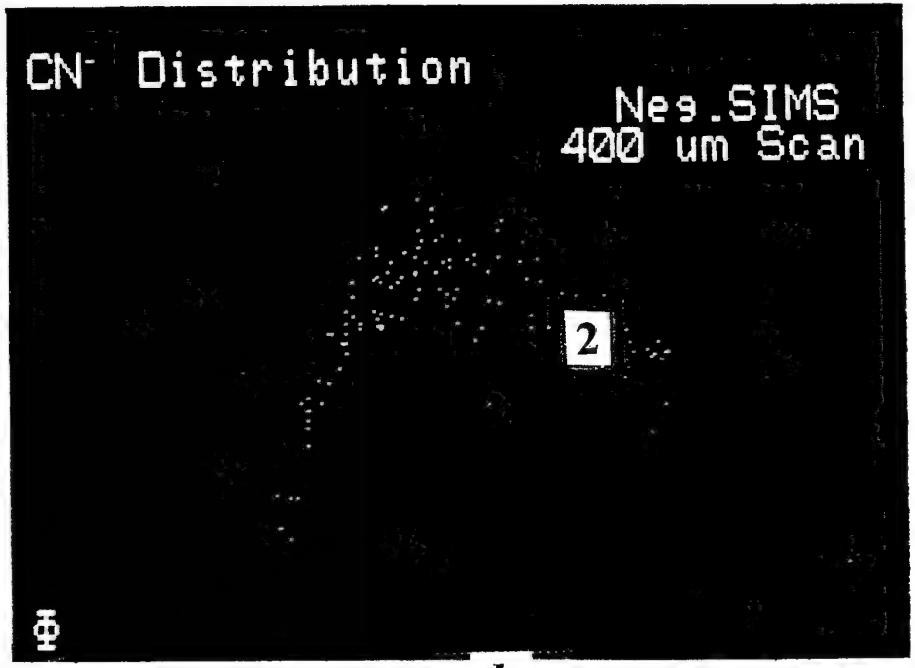
CN⁻ Distribution
Neg.SIMS
400 um Scan
2

d

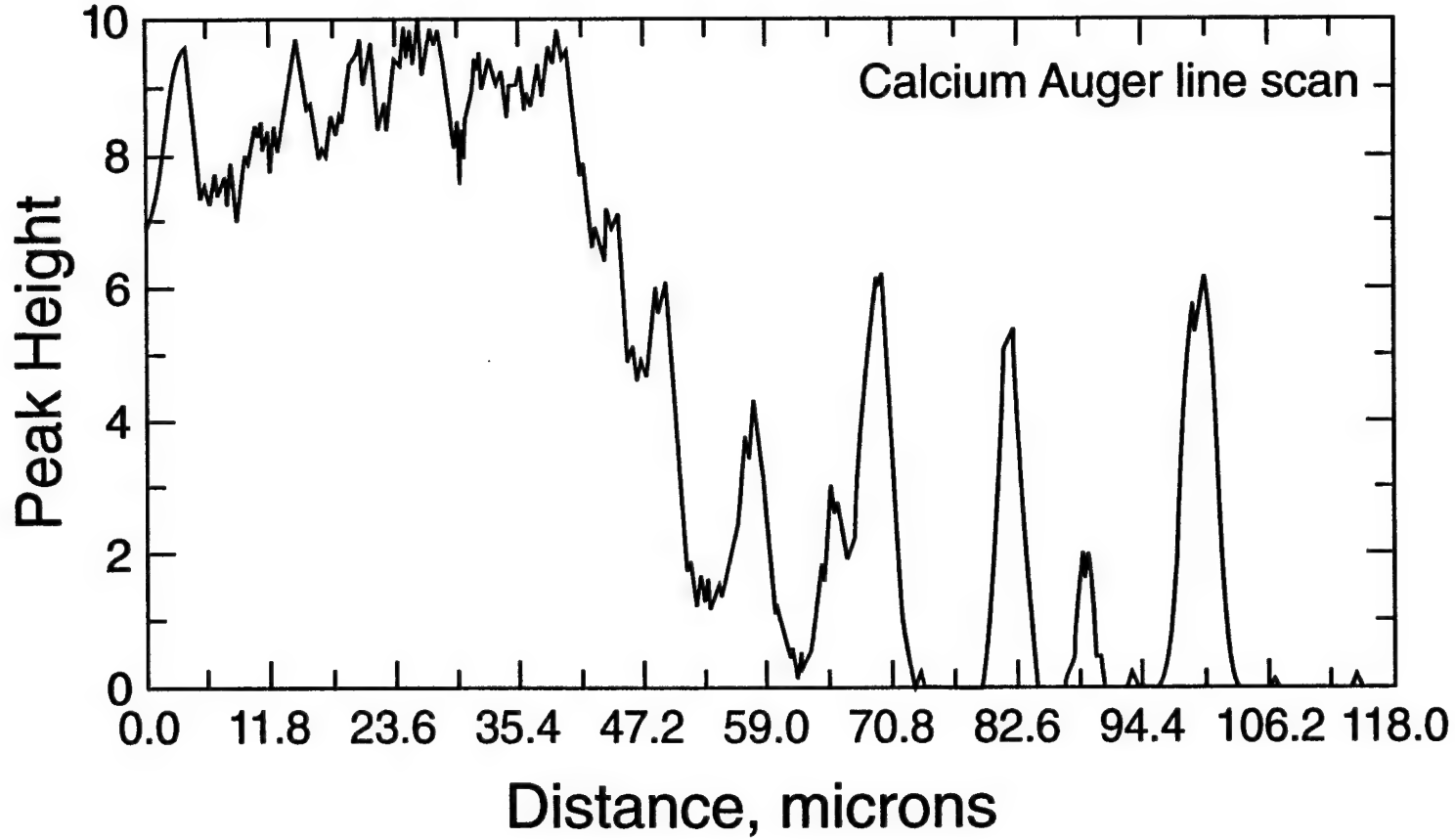

Schamberg 940363.39g

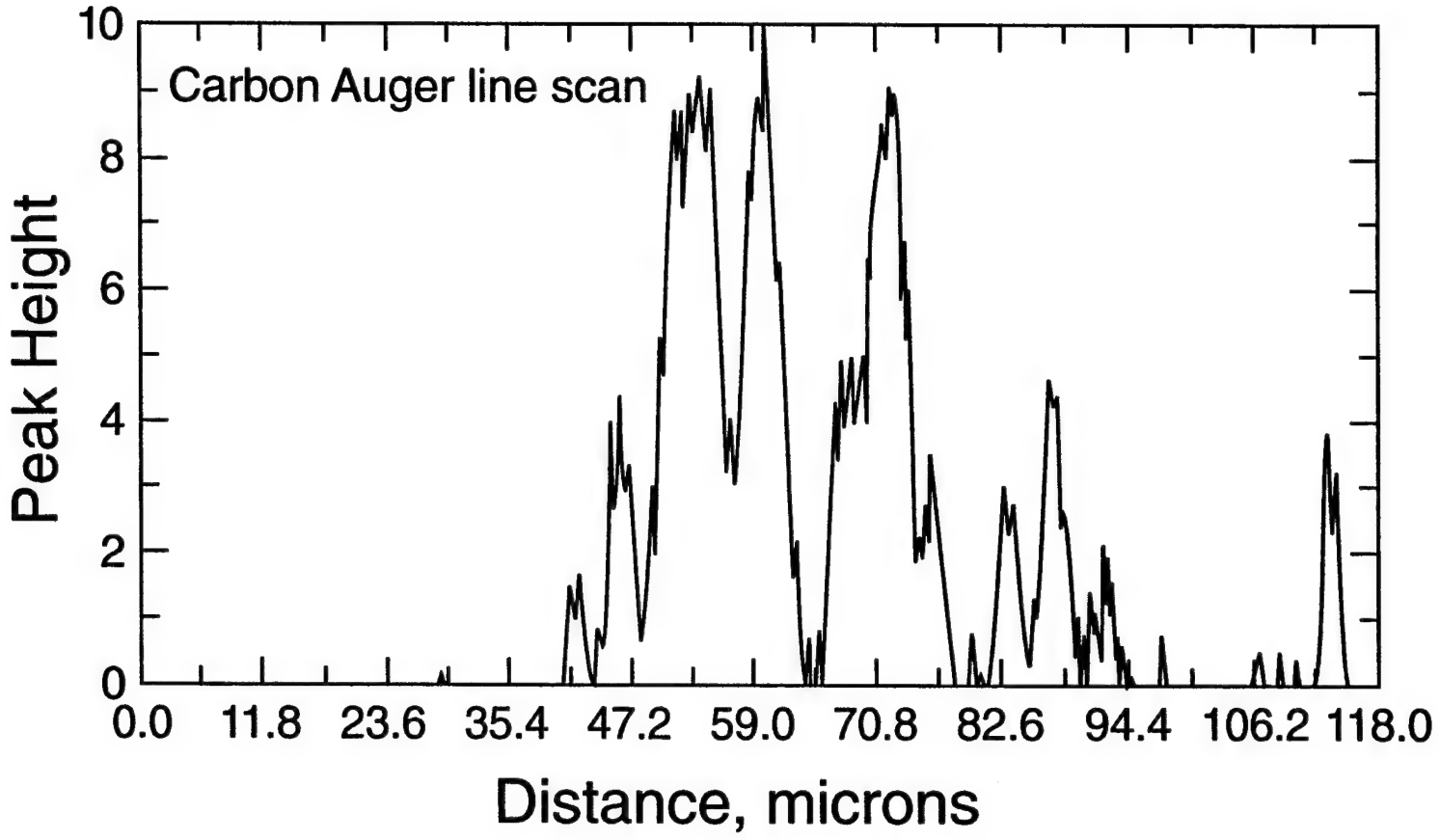
Carbon Auger line scan
Peak Height
10
8
6
4
2
0
0.0
11.8
23.6
35.4
47.2
59.0
70.8
82.6
94.4
106.2
118.0
Distance, microns

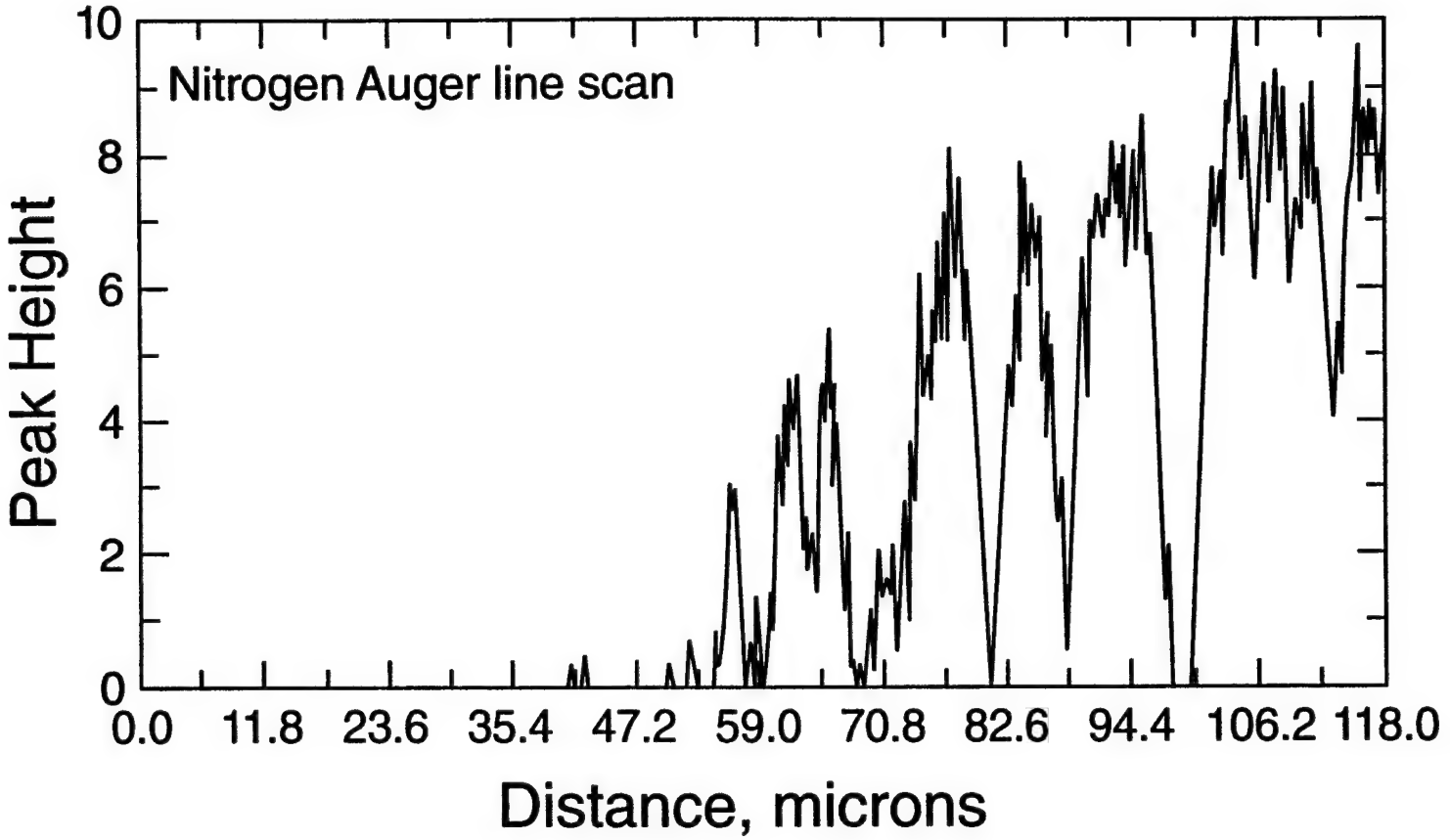

Schamberg 940363.41g

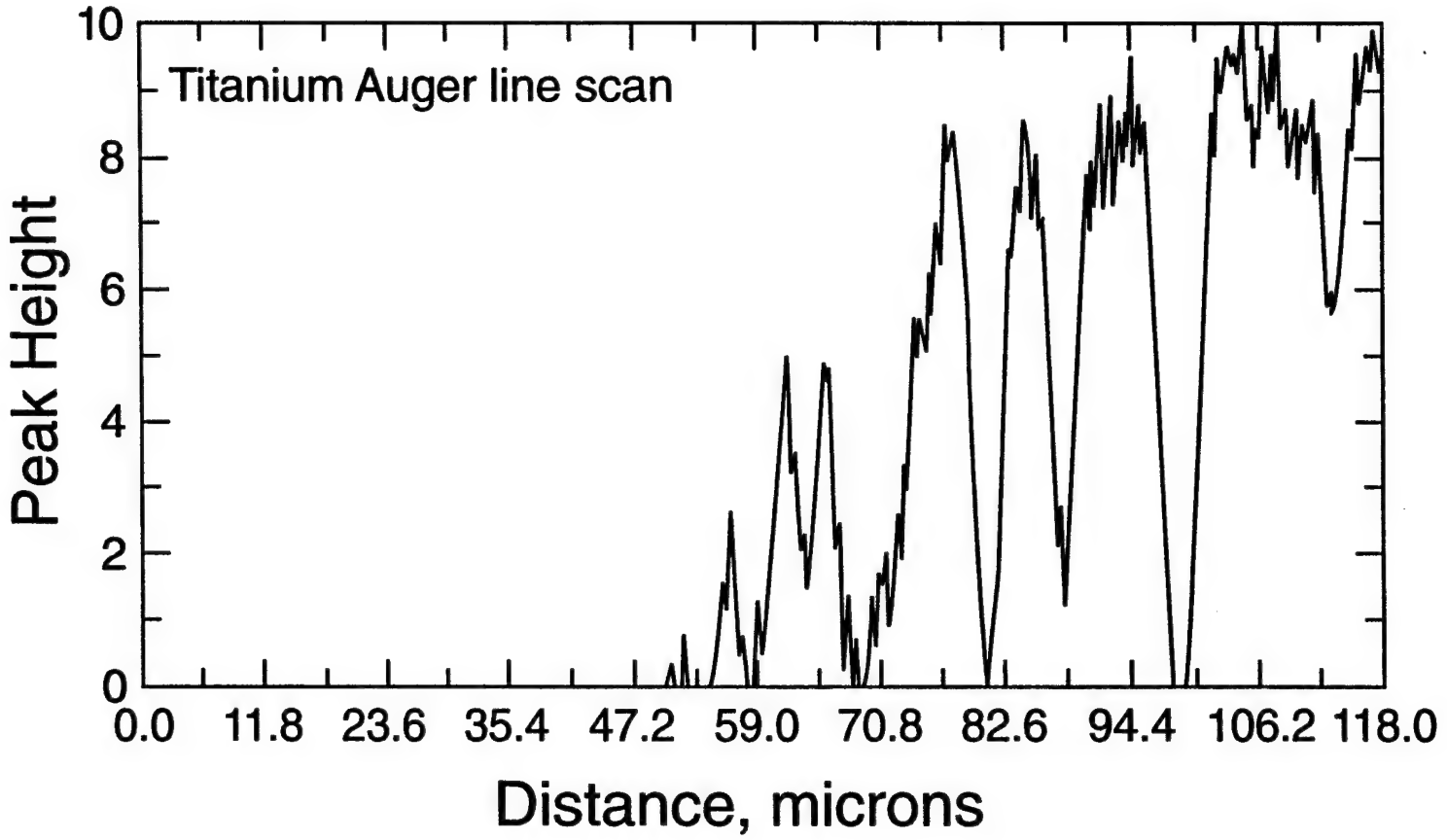

Schamberg 940363.42g

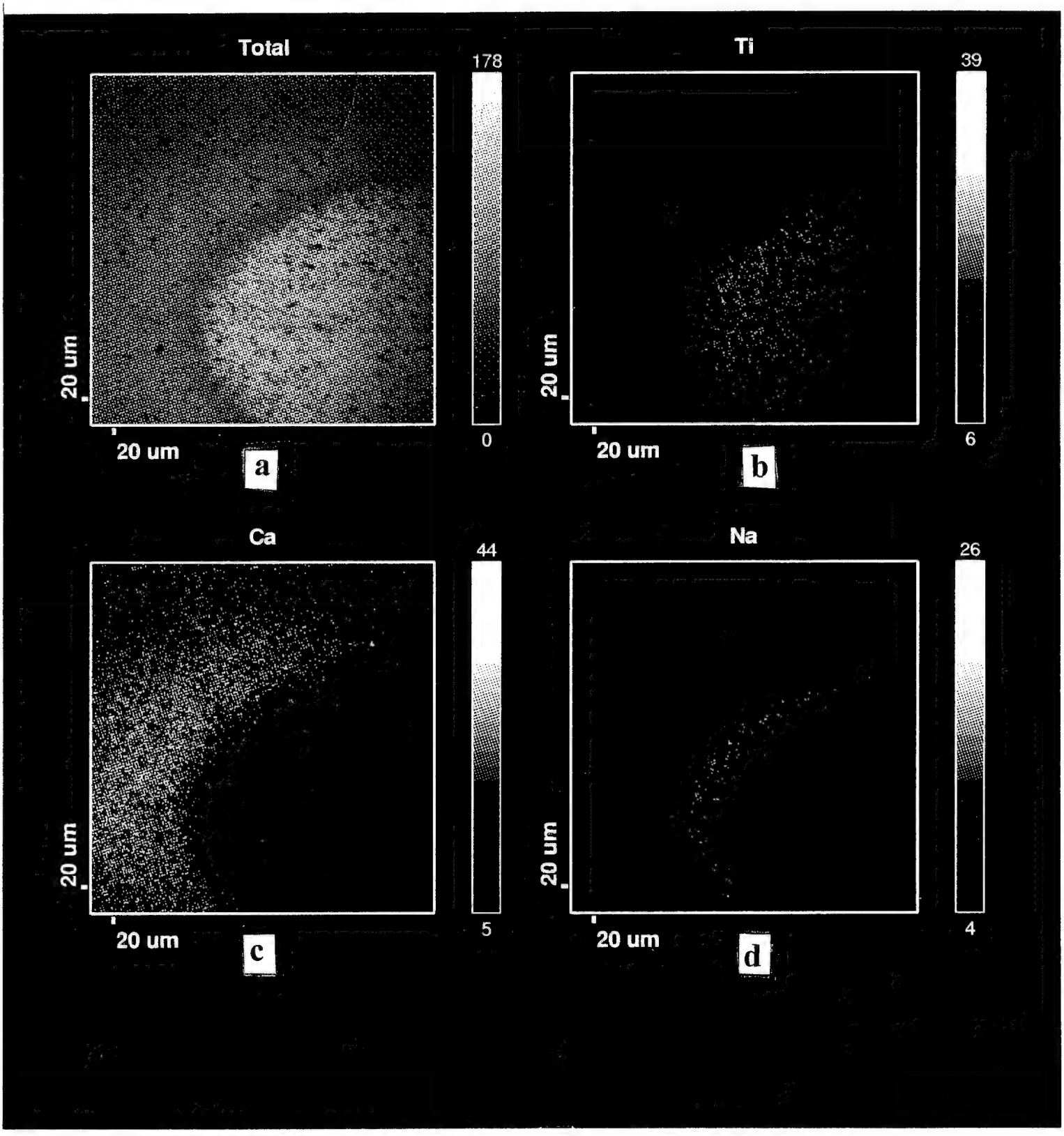
Total
178
0
20 um
20 um
a
Ti
39
6
20 um
20 um
b
Ca
44
5
20 um
20 um
c
Na
26
4
20 um
20 um
d

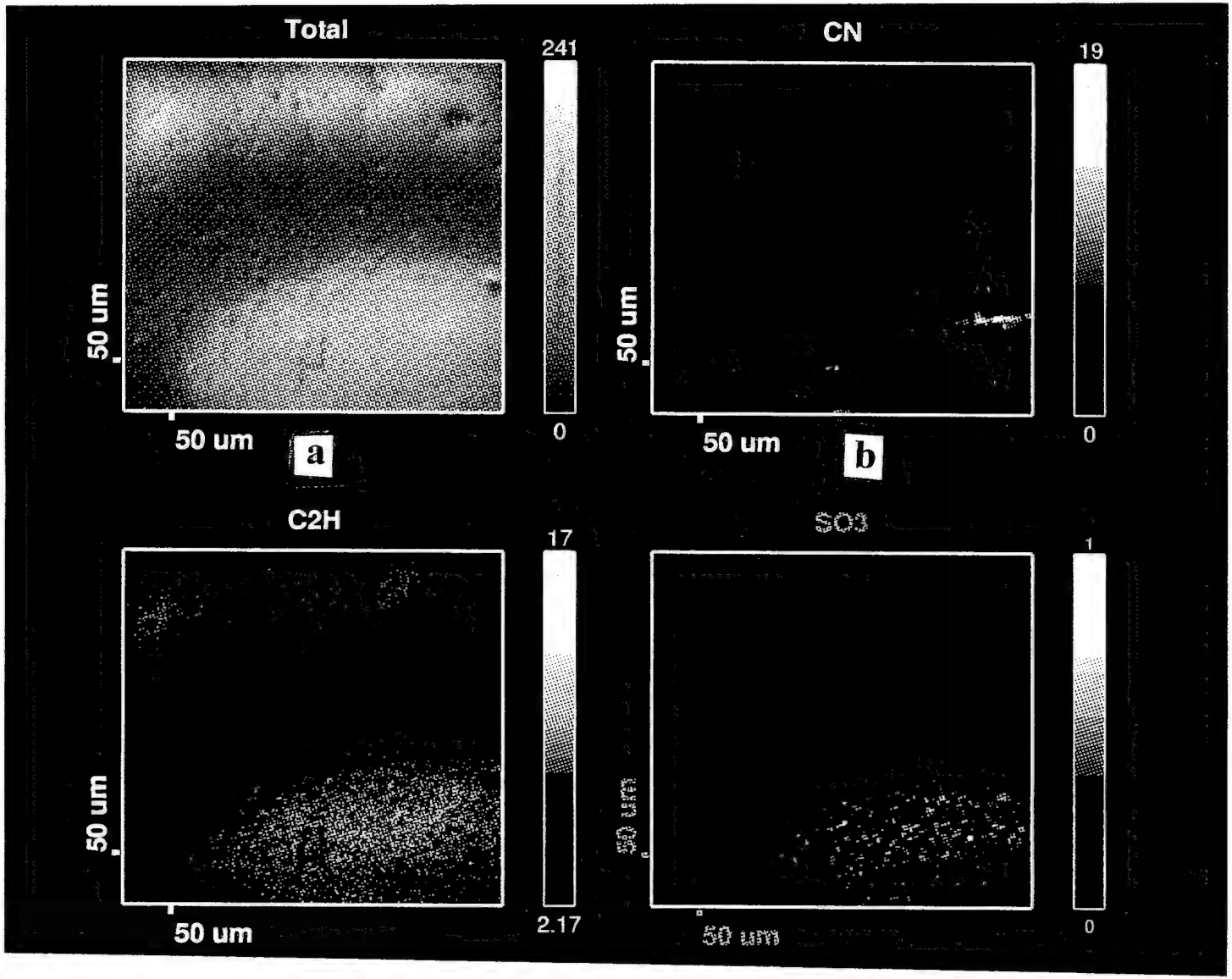
Total
241
0
50 um
50 um
a
CN
19
0
50 um
50 um
b
C2H
17
2.17
50 um
50 um
c
SO3
1
0
50 um
50 um
d

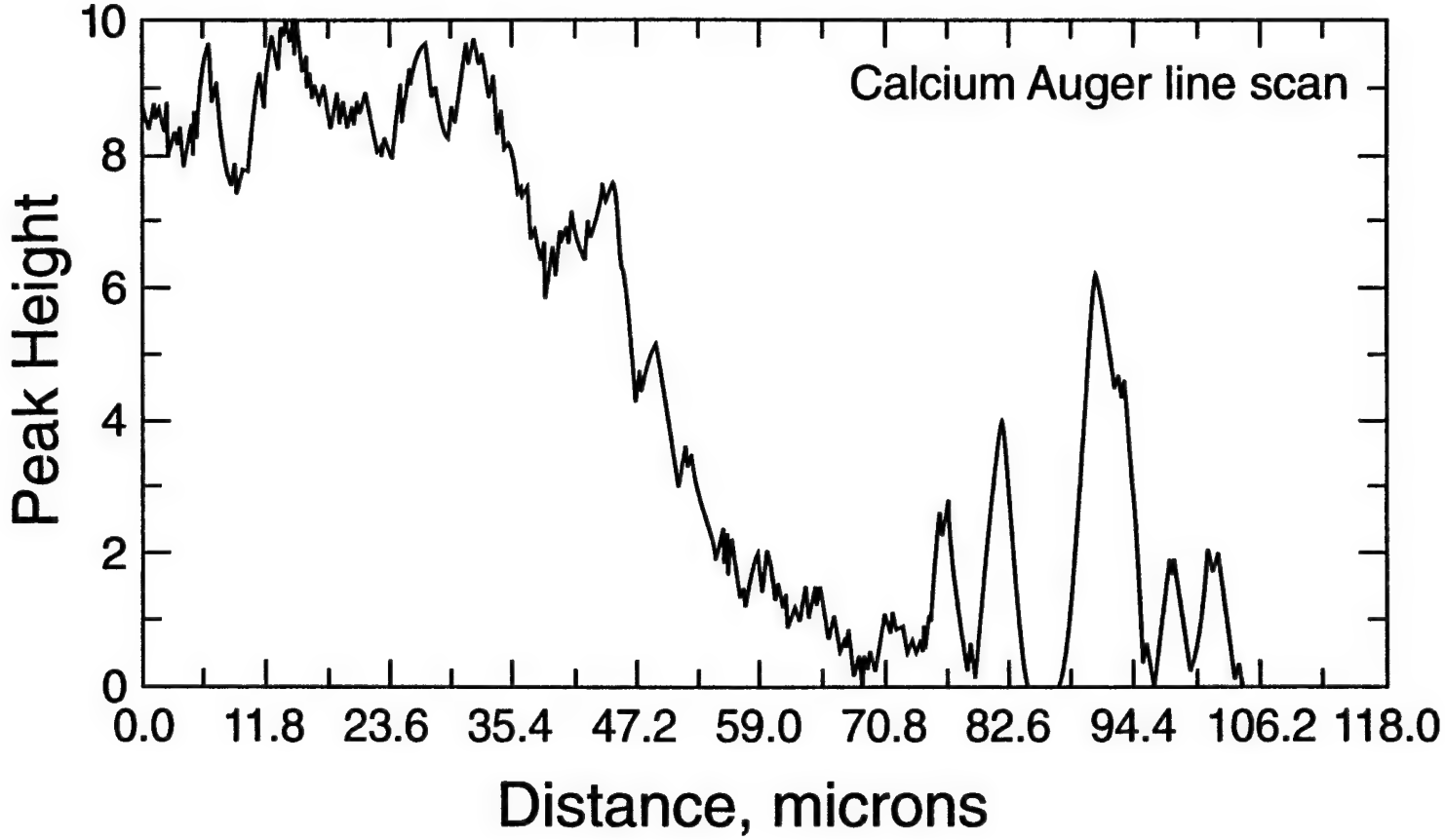

Schamberg 940363.43g

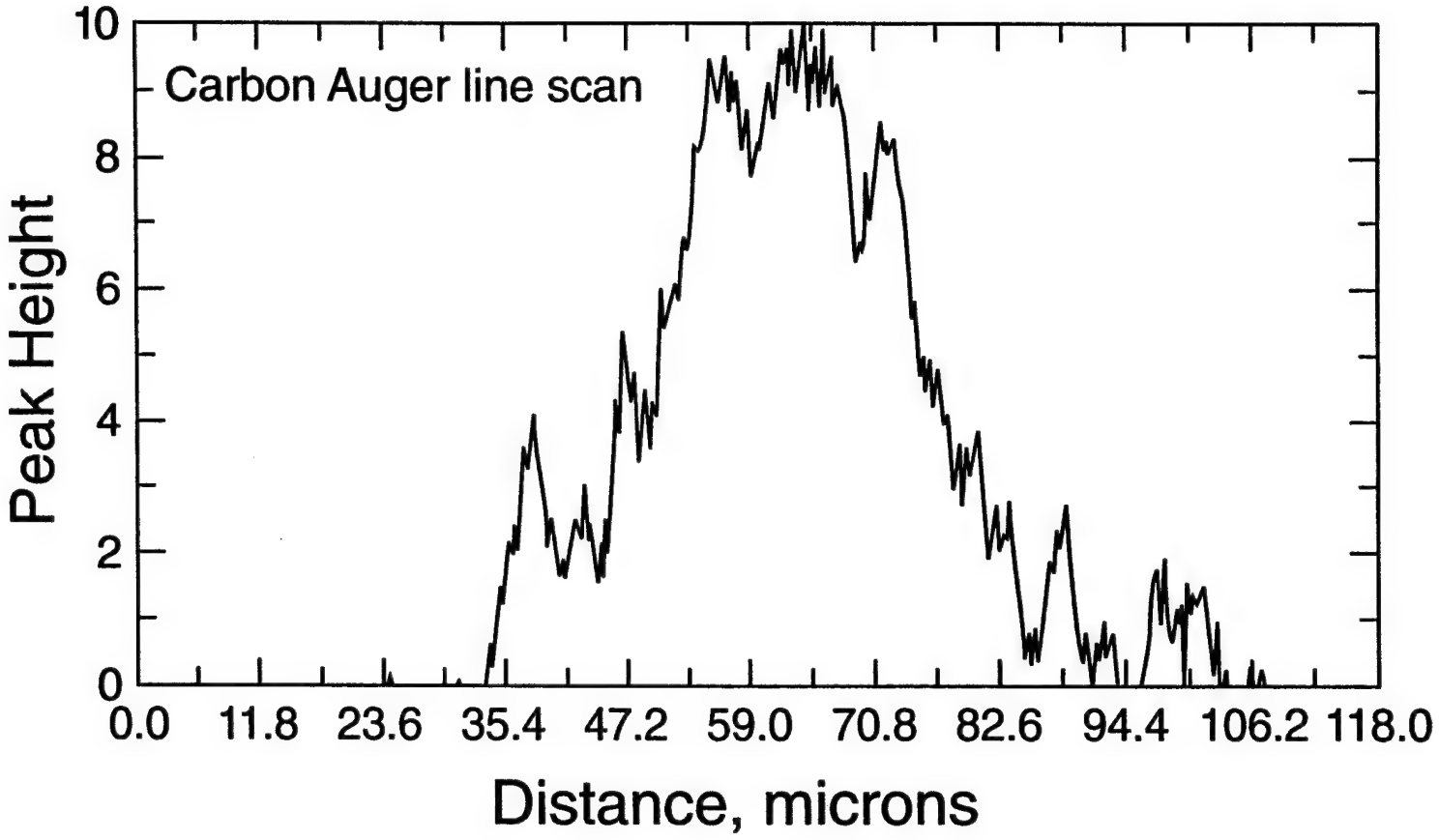

Schamberg 940363.44g

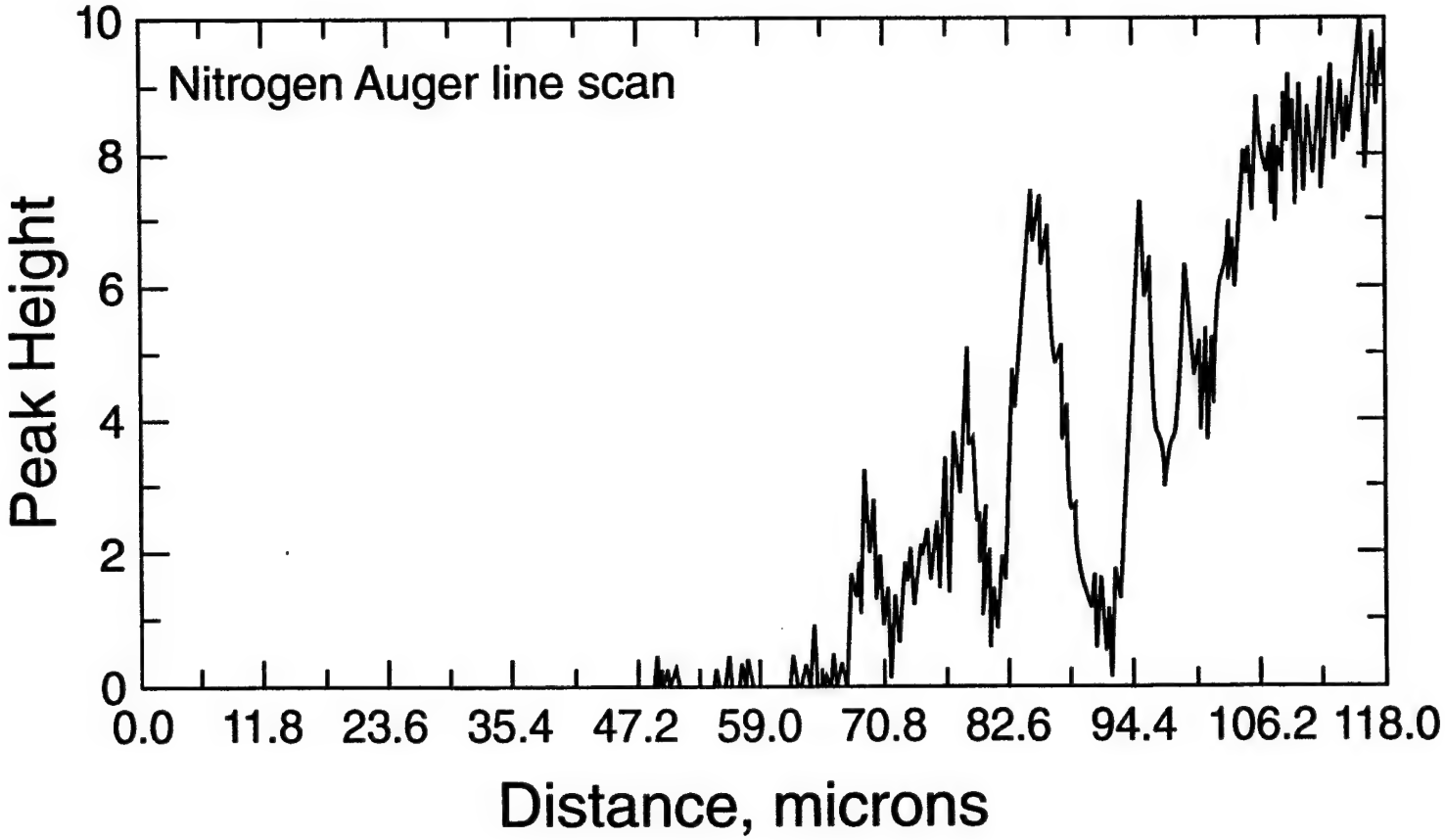
Nitrogen Auger line scan
Peak Height
10
8
6
4
2
0
0.0
11.8
23.6
35.4
47.2
59.0
70.8
82.6
94.4
106.2
118.0
Distance, microns

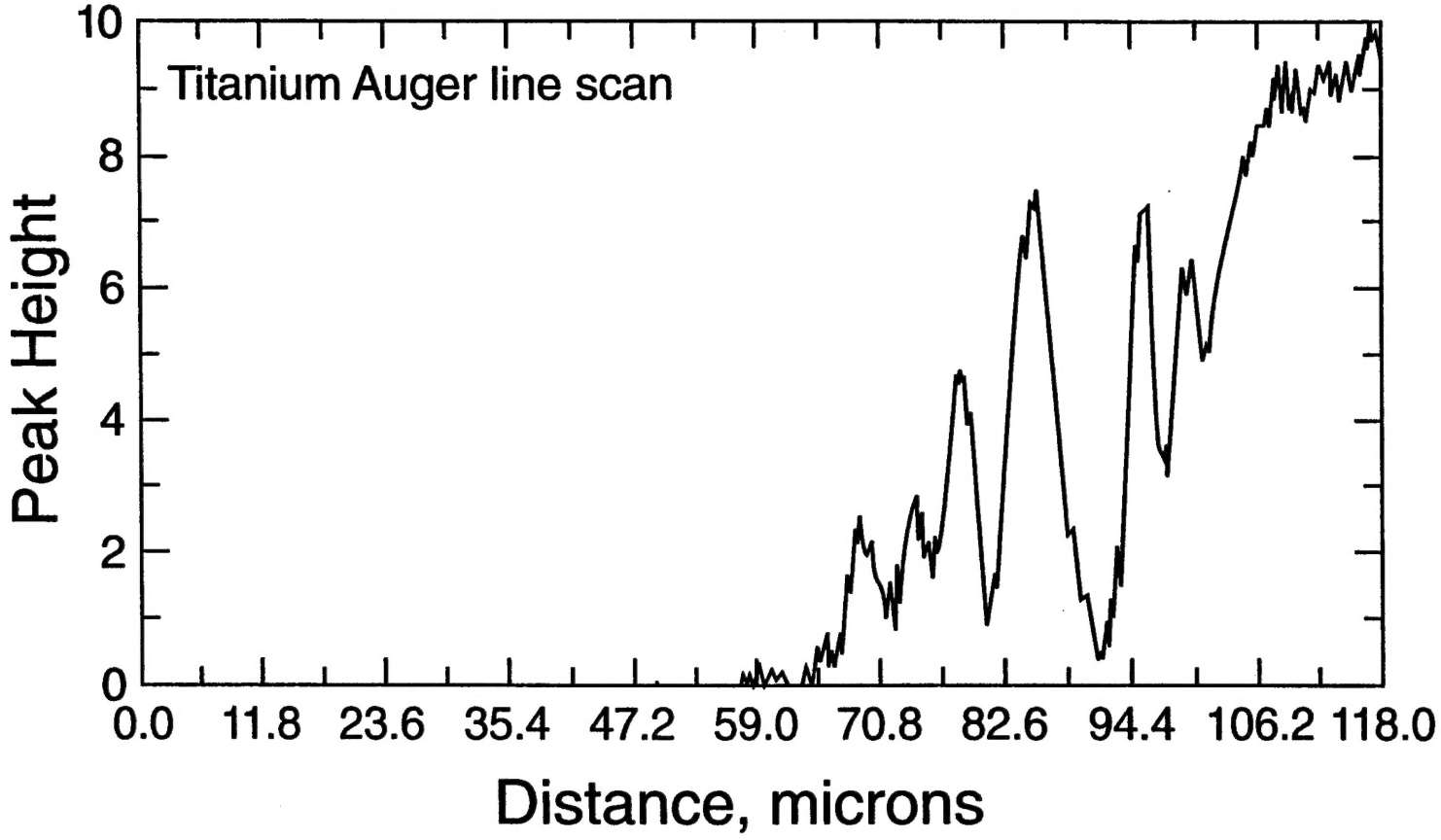

Schamberg 940363.46g

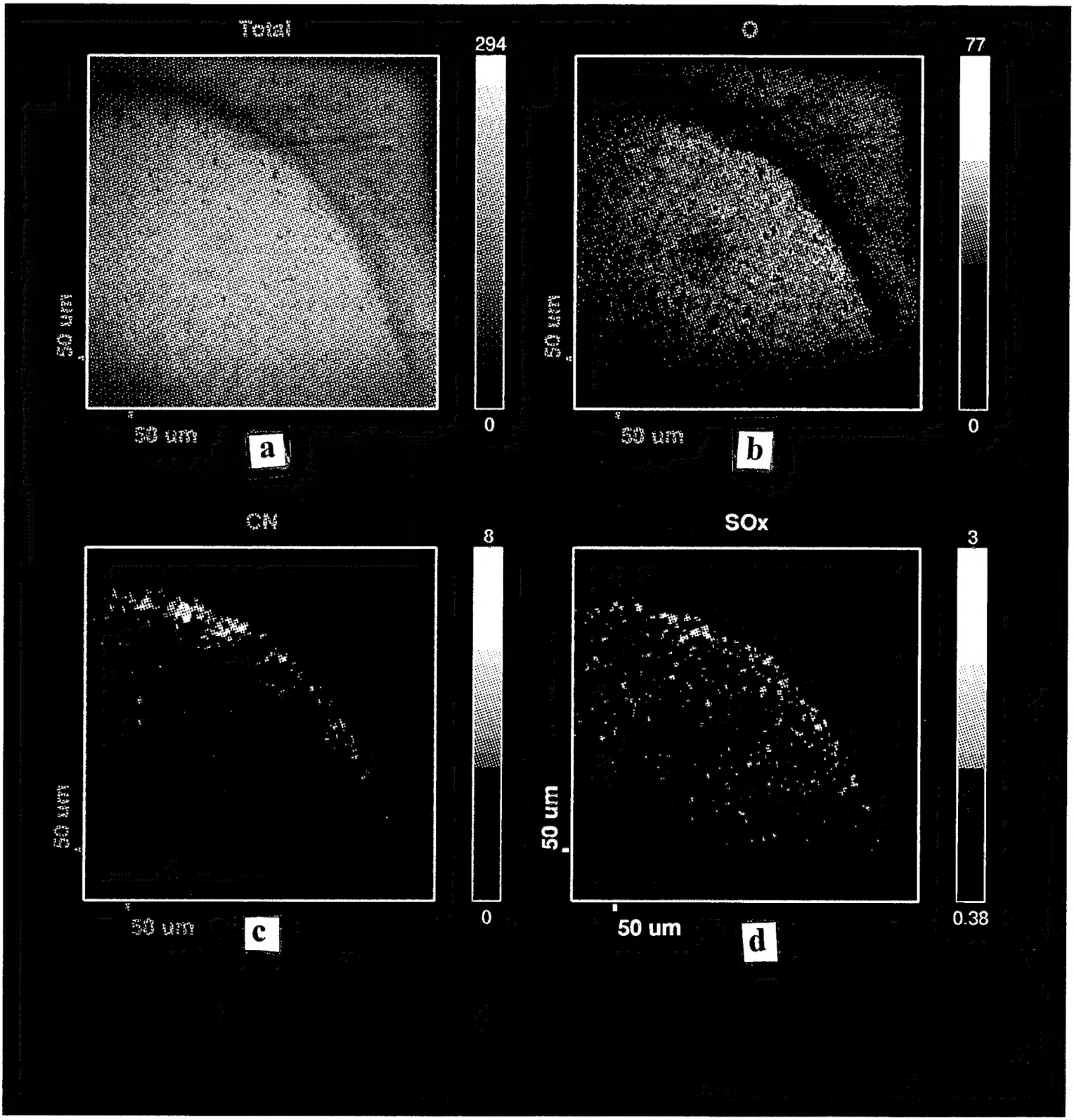
Total
294
0
50 um
50 um
a
O
77
0
50 um
50 um
b
CM
8
0
50 um
50 um
c
SOx
3
0.38
50 um
50 um
d

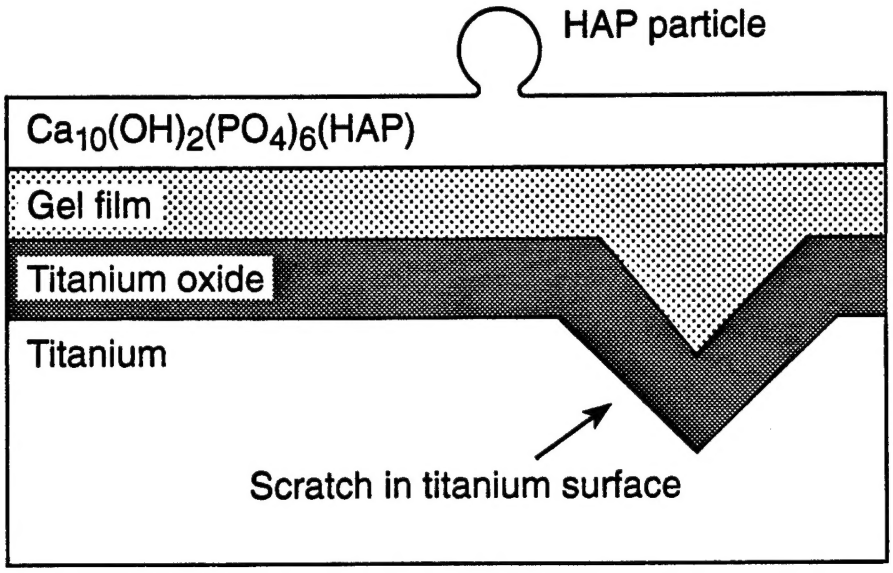

Before crater formation

Direction of line scan ⟶

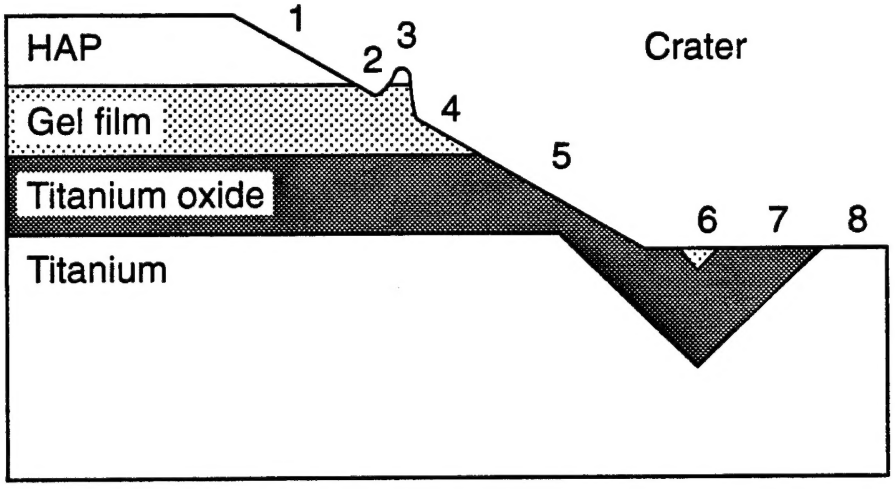

After crater formation

TECHNICAL REPORT DISTRIBUTION LIST - GENERAL

(For **complete** technical reports)

Office of Naval Research (1)*
Physical Science S & T Division 331
800 North Quincy Street
Arlington, VA 22217-5660

Defense Technical Information Center (2)
Building 5, Cameron Station
Alexandria, VA 22314

Dr. James S. Murday (1)
Chemistry Division, Code 6100
Naval Research Laboratory
Washington DC 20375-5342

Dr. John D. Fisher, Director (1)
Chemistry Division 474220D
Naval Air Warfare Center
Weapons Division
China Lake, CA 93555-6001

Dr. Peter Seligman (1)
NCCOSC RDT&E DIV 521
53475 Strothe Rd.
San Diego, CA 92152-6325

Dr. Richard W. Drisko (1)
Naval Facilities & Engineering
Service Center
Code L52
Port Hueneme, CA 93043

Dr. Eugene C. Fischer (1)
Code 2840
Naval Surface Weapons Center
Carderock Division Detachment
Annapolis, MD 21402-1198

Dr. Bernard E. Douda (1)
Crane Division
Naval Surface Warfare Center
Crane, Indiana 47522-5000

* *Number of copies to forward*